

MASTER OF SCIENCE THESIS

# Effect of Ambient Temperature on Fatigue Delamination Growth in Composite Laminates

M. Beyens

Faculty of Aerospace Engineering · Delft University of Technology



# **Effect of Ambient Temperature on Fatigue Delamination Growth in Composite Laminates**

MASTER OF SCIENCE THESIS

For obtaining the degree of Master of Science in Aerospace Engineering  
at Delft University of Technology

M. Beyens

August 27th 2021



Copyright © M. Beyens  
All rights reserved.

DELFT UNIVERSITY OF TECHNOLOGY  
FACULTY OF AEROSPACE ENGINEERING  
DEPARTMENT OF AEROSPACE STRUCTURES AND MATERIALS

**GRADUATION COMMITTEE**

Dated: August 27th 2021

Chair holder:

---

Supervisor: Dr. ir. R. C. Alderliesten

Committee members:

---

Ir. J. Sinke

---

Dr.ir. J. A. Pascoe

---

Dr.ir. L. Yao



---

# Preface

This report describes the research I have done during my master thesis on the subject of the effect of temperature on fatigue delamination growth. It is the result of a thorough literature study and an extensive experimental campaign under supervision of René Alderliesten and Liaojun Yao. This report informs the reader about the process I have followed as well as the results I have obtained.

This master thesis report would not have been possible without the support of several people. Firstly, the technicians of Delft Aerospace Structures and Materials Laboratory Fred Bosch, Victor Horbowiec, Johan Boender, Berthil Grashof, Dave Ruijtenbeek and Alexander Uithol. Thank you to Dimitrios Zarouchas for his help with the acoustic emission equipment. Special thanks go out to Roberto Motta for his advice and support on both practical and theoretical matters.

Thank you to my second supervisor Liaojun Yao for the fruitful discussions and feedback I have received during my master thesis. Finally, my deepest gratitude goes out to my first supervisor René Alderliesten for his help, guidance, discussions and feedback.



---

# Abstract

Since composites were first introduced in aircraft in the 1950s, their usage has increased. Nowadays, aircraft are built in which 50% of their weight is composite materials. Using composites brings along a whole new set of challenges, among which damage is one of the most critical. Because damage in composites is often not visible, a good understanding of the damage phenomena is necessary. This research project focused on delamination growth in composite laminates and helps fill the knowledge gap in the understanding of the influence of temperatures on several delamination growth parameters. Experiments were performed at  $-40^{\circ}\text{C}$ , room temperature,  $50^{\circ}\text{C}$  and  $80^{\circ}\text{C}$  to cover a temperature interval relevant to aircraft.

The effect of temperature on three fatigue delamination growth parameters was focused on. These are: fatigue delamination growth excluding fibre bridging, fibre bridging and the stress-ratio effect. The fatigue delamination growth rate was found to decrease with decreasing temperature when excluding fibre bridging. The effect of temperature on fibre bridging was the opposite. When including fibre bridging, the fatigue delamination growth rate increased with decreasing temperature. The effect fibre bridging has on fatigue delamination growth becomes larger at higher temperatures. Fatigue delamination growth decreases with decreasing stress ratio. When excluding fibre bridging, this decrease becomes larger with decreasing temperature. When taking fibre bridging into account, the decrease was larger towards both extremities of the temperature interval.



---

# Table of Contents

<b>1</b>	<b>Introduction</b>	<b>1</b>
<b>2</b>	<b>Literature Review</b>	<b>3</b>
2.1	Questions to the literature . . . . .	3
2.2	What temperature range is relevant to be investigated during the experimental campaign? . . . . .	4
2.3	What influence has temperature on the material properties? . . . . .	5
2.4	How do fracture mechanics apply to fatigue delamination growth in composite laminates? . . . . .	6
2.4.1	Strain Energy Release Rate and Stress Intensity Factor . . . . .	6
2.4.2	Similitude parameters . . . . .	7
2.4.3	Paris relation . . . . .	8
2.5	How do energy principles provide a physical approach to fatigue delamination growth in composite laminates? . . . . .	8
2.6	What are the critical parameters for fatigue delamination growth at room temperature? . . . . .	10
2.6.1	Stress ratio effect . . . . .	10
2.6.2	fibre bridging . . . . .	11
2.7	What is the effect of temperature on fatigue delamination growth? . . . . .	14
<b>3</b>	<b>Research Questions</b>	<b>17</b>
<b>4</b>	<b>Methodology</b>	<b>19</b>
4.1	Material and Specimen Manufacturing . . . . .	19
4.2	Experimental Campaign and Test Setup . . . . .	21
4.2.1	Experimental Campaign . . . . .	21
4.2.2	Quasi-static Test Campaign . . . . .	21
4.2.3	Fatigue Test Campaign . . . . .	22

4.2.4	List of Experiments . . . . .	23
4.2.5	Test Setup . . . . .	23
4.3	Data Analysis . . . . .	25
4.4	Data Representation . . . . .	26
<b>5</b>	<b>Results</b>	<b>29</b>
5.1	Room Temperature Data . . . . .	29
5.1.1	Quasi-static Data . . . . .	29
5.1.2	Fatigue Data at a Stress Ratio of 0.1 . . . . .	30
5.1.3	Fatigue Data at Stress Ratio of 0.5 . . . . .	32
5.1.4	Concluding remarks . . . . .	33
5.2	Temperature Influence on Delamination Resistance . . . . .	33
5.3	Temperature Influence on Fibre Bridging . . . . .	37
5.3.1	Fibre Bridging at -40°C . . . . .	37
5.3.2	Fibre Bridging at 50°C . . . . .	40
5.3.3	Fibre Bridging at 80°C . . . . .	43
5.3.4	Temperature comparison . . . . .	45
5.4	Temperature Influence on the Stress Ratio Effect . . . . .	48
<b>6</b>	<b>Discussion</b>	<b>53</b>
6.1	Room Temperature Data . . . . .	53
6.1.1	Quasi-static data . . . . .	53
6.1.2	Fatigue data at a stress ratio of 0.1 . . . . .	56
6.1.3	Fatigue data at a stress ratio of 0.5 . . . . .	57
6.1.4	Concluding statements . . . . .	58
6.2	Temperature Influence on Delamination Resistance . . . . .	59
6.3	Temperature Influence on Fibre Bridging . . . . .	59
6.4	Temperature Influence on Stress Ratio Effect . . . . .	60
6.5	Temperature influence on fatigue delamination growth . . . . .	61
<b>7</b>	<b>Conclusions and recommendations</b>	<b>63</b>
7.1	Conclusions . . . . .	63
7.2	Recommendations . . . . .	64
	<b>References</b>	<b>64</b>
	References	65
<b>A</b>	<b>List of experiments</b>	<b>71</b>

---

## List of Figures

4.1	Autoclave curing procedure . . . . .	20
4.2	DCB specimen; Figure taken from [1] and modified to personal need . . . . .	20
4.3	experimental setup for DCB testing at different temperatures . . . . .	24
4.4	detail from experimental setup for DCB testing at different temperatures depicting the test specimen attached to the fatigue machine . . . . .	24
4.5	$\Delta G$ vs $da/dN$ graph of six tests on a specimen at $R = 0.1$ and $T = 50^\circ\text{C}$ . . . . .	26
4.6	$\Delta G$ vs $da/dN$ graph of six tests on a specimen at $R = 0.1$ and $T = 50^\circ\text{C}$ comparing different amounts of data points . . . . .	27
4.7	$\Delta G$ vs $da/dN$ graph of six tests on a specimen at $R = 0.1$ and $T = 50^\circ\text{C}$ using one in every five datapoints . . . . .	27
5.1	Force-displacement graph for quasi-static tests at room temperature . . . . .	30
5.2	resistance curves for quasi-static tests at room temperature . . . . .	30
5.3	R-curves for tests F0.1_UD_RT_01 and F0.1_UD_RT_02 with $R = 0.1$ and $T =$ room temperature at $da/dN = 1\text{E-}7$ . . . . .	31
5.4	resistance curves for test F0.1_UD_RT_01 with $R = 0.1$ and $T =$ room temperature at different precrack lengths . . . . .	31
5.5	resistance curves for test F0.1_UD_RT_02 with $R = 0.1$ and $T =$ room temperature at different precrack lengths; note: the resistance curve with precrack length of 14mm is out of place compared to the other resistance curves. This is due to a machine malfunction halfway through the test. . . . .	32
5.6	R-curves for tests F0.5_UD_RT_01 and F0.5_UD_RT_02 with $R = 0.5$ and $T =$ room temperature at $da/dN = 1\text{E-}7$ . . . . .	32
5.7	resistance curves for test F0.5_UD_RT_02 with $R = 0.5$ and $T =$ room temperature at different precrack lengths . . . . .	33
5.8	Comparison between resistance curves and the corresponding zero bridging curve for test F0.1_UD_50_02 with $R = 0.1$ and $T = 50^\circ\text{C}$ . . . . .	34
5.9	$\Delta G$ vs $da/dN$ zero bridging curves at different temperatures . . . . .	34
5.10	$\Delta G$ vs $da/dN$ zero bridging curves at different temperatures . . . . .	35

5.11	da/dN vs dU/dN graph with left zero bridging boundary and right maximum bridging boundary . . . . .	36
5.12	dU/dN vs da/dN zero bridging curves at different temperatures . . . . .	36
5.13	Resistance curves of test F0.1_UD_-40_01 carried out at -40°C with a stress ratio of 0.1 with different fatigue precrack lengths . . . . .	37
5.14	Comparison between zero bridging curve and resistance curve at certain fatigue precrack lengths . . . . .	38
5.15	Quasi-static resistance curve and fatigue R-curve at a da/dN value of 1E-7 . . . . .	38
5.16	Resistance curves of test F0.1_UD_-40_01 carried out at -40°C with a stress ratio of 0.1 with different fatigue precrack lengths . . . . .	39
5.17	Resistance curves of test F0.1_UD_50_02 carried out at 50°C with a stress ratio of 0.1 with different fatigue precrack lengths . . . . .	41
5.18	Comparison between zero bridging curves and resistance curves of test F0.1_UD_50_02 at certain fatigue precrack lengths . . . . .	41
5.19	Quasi-static resistance curve and fatigue R-curve at a da/dN value of 1E-7 . . . . .	42
5.20	Resistance curves of test F0.1_UD_50_02 carried out at 50°C with a stress ratio of 0.1 with different fatigue precrack lengths . . . . .	42
5.21	Resistance curves of test F0.1_UD_80_01 carried out at -40°C with a stress ratio of 0.1 with different fatigue precrack lengths . . . . .	43
5.22	Comparison between zero bridging curves and resistance curves of test F0.1_UD_80_01 at certain fatigue precrack lengths . . . . .	44
5.23	Quasi-static resistance curve and fatigue R-curve at a da/dN value of 1E-7 . . . . .	44
5.24	Resistance curves of test F0.1_UD_80_01 carried out at 80°C with a stress ratio of 0.1 with different fatigue precrack lengths . . . . .	45
5.25	Temperature comparison of resistance curves with fatigue precrack lengths between 31mm and 42mm with their corresponding zero bridging curves . . . . .	46
5.26	Temperature comparison of resistance curves with fatigue precrack lengths between 90mm and 103mm with their corresponding zero bridging curves . . . . .	46
5.27	Temperature comparison of fatigue R-curves at a da/dN value of 1E-7 . . . . .	47
5.28	Temperature comparison of fatigue resistance curves at zero bridging and maximum bridging using energy principles . . . . .	47
5.29	Temperature comparison of zero bridging resistance curves at stress ratio 0.1 and stress ratio 0.5 . . . . .	48
5.30	Temperature comparison of zero bridging resistance curves at stress ratio 0.1 and stress ratio 0.5 . . . . .	49
5.31	Temperature comparison of resistance curves with fatigue precrack lengths between 90mm and 103mm with their corresponding zero bridging curves at stress ratio 0.1 and stress ratio 0.5 . . . . .	49
5.32	temperature comparison of fatigue resistance curves at zero bridging using energy principles at stress ratio 0.1 and stress ratio 0.5 . . . . .	50
5.33	temperature comparison comparison of fatigue resistance curves at maximum using energy principles at stress ratio 0.1 and stress ratio 0.5 . . . . .	51
6.1	Force displacement curves of all QS tests performed at room temperature and of tests performed by Yao . . . . .	54
6.2	Quasi-static resistance curves of all QS tests performed at room temperature and of tests performed by Yao . . . . .	54

---

6.3	Side view of a specimen tested during the experimental phase of this research project showing signs of fibre bridging . . . . .	55
6.4	Side view of a specimen tested by Yao showing signs of fibre bridging . . . . .	55
6.5	Resistance curve of fatigue tests specimen 7 and F0.1_UD_RT_02 at stress ratio 0.5 with different fatigue precrack lengths . . . . .	56
6.6	R-curve of fatigue tests specimen 7 and F0.1_UD_RT_02 at stress ratio 0.5 and $da/dN$ of $1.0E-7$ . . . . .	57
6.7	Resistance curve of fatigue tests specimen 10 and F0.2_UD_RT_02 at stress ratio 0.1 with different fatigue precrack lengths . . . . .	58



---

# List of Tables

4.1	Elastic properties of the prepreg M30SC/DT120 [2]	19
4.2	Quasi-static test campaign	22
4.3	Fatigue test campaign	23
A.1	List of all experiments performed in this research project	72



---

# Chapter 1

---

## Introduction

In the 1950s, glass-fibre composites were first used in aircraft [3]. Over the past decades, more and more glass-fibre, carbon-fibre and other types of composites have been used in the aircraft industry. A major advantage of composites is that they can be tailored for very specific load cases in different parts of a structure. This, combined with their high specific strength properties aids to decreasing the weight of an aircraft compared to their aluminium counterparts. This increase in composite use is most visible in the Boeing 787 and the Airbus A350. Their weight consist for more than 50% out of composites [4, 5].

This use of new materials also brings along a whole new set of challenges among which damage is one of the most critical. Metals show signs of yielding before failure whereas composites appear to be damage-free until the point of final failure. Because damage in composites is often not visible, a good understanding of the damage phenomena is necessary to be able to predict failure. The research in this report focuses on fatigue delamination, which is an internal damage type and thus difficult to detect. For this research, a distinction is made between a crack and delamination. A crack can occur in the material, sometimes at a flaw in the material, under loading [6]. A delamination is a specific type of crack in which two layers of the composite material come apart [7].

The purpose of this report is to explain how the research project took place, what the outcome is and to ultimately answer the research question "What is the effect of ambient temperature on fatigue delamination growth in composite laminates?".

The report is structured as follows. In Chapter 2, a review of the literature regarding the subject of fatigue delamination growth is given based on questions that are asked to the literature. In Chapter 3, the research questions that have to be answered in the research project are posed. Chapter 4 gives an overview of the methodology used during preparation and testing as well as during data analysis. Then, the results of the data analysis are given in Chapter 5 after which the results are discussed in Chapter 6. Finally, Conclusions are drawn and recommendations are given in Chapter 7.



---

## Chapter 2

---

# Literature Review

In this chapter, a review of the literature on previous work in the domain of fatigue delamination growth is presented. This is done based on questions that are asked to the literature. Those questions are given in Section 2.1. In Sections 2.2 through 2.7, these questions are answered.

### 2.1 Questions to the literature

The literature review was performed based on a set of questions that were asked to the literature. These questions were set up with the goal of obtaining information that is relevant to have when planning and developing the test campaign and performing and analysing the tests and results during the experimental phase of this project. The questions on which the literature review is based are the following:

1. What temperature range is relevant to be investigated during the experimental campaign?
2. What influence has temperature on the material properties?
3. How do fracture mechanics apply to fatigue delamination growth in composite laminates?
4. How do energy principles provide a physical approach to fatigue delamination growth in composite laminates?
5. What are the critical parameters for fatigue delamination growth at room temperature?
6. What is the effect of temperature on fatigue delamination growth?

The first question aims at researching what temperatures occur in the operating life of composites in aircraft and what temperature ranges have been used in previous research where the ambient temperature effects on aerospace composites have been researched.

With answering the second research question, the temperature effects on the material properties are researched. The effect on the matrix, the fibres and the fibre-matrix interaction is looked at. This can provide insight in the behavior of the material at different temperatures. Although the main focus of this research is on finding physics based explanations, studying the underlying theory is necessary and can be used in combination with physical observations to create a physics based model. Therefore, question three will focus on the application of fracture mechanics on fatigue delamination growth.

Because this research focuses on finding physics based explanations, the fourth question will look at how energy principles can provide a physical approach to fatigue delamination growth. Answering the fifth question will provide knowledge on the critical parameters for fatigue delamination growth at room temperature. These are the stress ratio effect and fibre bridging. When the effect of these parameters at room temperature is known, it allows to see how this effect changes with temperature.

Finally, the sixth question focuses on the effect of temperature on fatigue delamination growth by reviewing past research on the topic. This research can be used to have an estimate of what will happen at the different temperatures.

In the following sections, answers to these questions will be given based on literature.

## 2.2 What temperature range is relevant to be investigated during the experimental campaign?

When investigating the effect of ambient temperature on fatigue delamination growth in composite laminates, it is important to determine a temperature range that is representative for conditions that can occur in the life of an aircraft. In general, a temperature range of about  $-50^{\circ}\text{C}$  to  $80^{\circ}\text{C}$  is assumed to be a good range of temperatures that are relevant for the aircraft industry, not taking into account temperatures that occur in the engines. Although no specific sources are given that support this assumption, it is widely adopted [8, 9]. It is however worthwhile to have a closer look at where this temperature range originates from.

Several factors can play a role in the temperature that is experienced by the material in an aircraft structure. First there is the air temperature, both at ground level and at cruise altitude. At cruise altitude, air temperature is about  $-55^{\circ}\text{C}$  [10]. At ground level, temperatures vary much more. The hottest air temperature recorded at an airport is  $54^{\circ}\text{C}$  [11, 12] whereas the coldest is  $-39^{\circ}\text{C}$  [11]. These temperatures were recorded at Ahvaz international airport in Iran and Yakutsk airport in Russia respectively.

A factor that can have influence on the skin temperature of an aircraft is the color of paint that is used. Darker colours absorb more heat than lighter colours. From the data collected by R. Levinson et al. [13] for their research on the potential benefits of solar reflective car shells, it could be deduced that after one hour in the sun, the roof surface of a black car reached 1.9 times the air temperature whereas the roof surface of a lighter, silver, coloured car reached 1.55 times the air temperature. This would mean that the skin temperature of a black aircraft parked for one hour at Ahvaz airport could reach as high as  $102^{\circ}\text{C}$ .

Finally, there are also dynamic factors like aerodynamic friction heating that can affect material temperature. However, this influence is only relevant in high speed flight [14, 15].

When putting this information together, the generally assumed temperature range of  $-50^{\circ}\text{C}$  to  $80^{\circ}\text{C}$  is a good fit.

In order to validate the use of this temperature range, previous studies on temperature effects are used. In a study of the temperature influence on interlaminar fracture toughness in carbon-epoxy composites by Sales et al. [16], a temperature range from  $-54^{\circ}\text{C}$  to  $80^{\circ}\text{C}$  is used. They claim that this range of temperatures is *'equivalent to those that the composites are subjected to whilst in service'* without supporting this claim with references or any sort of reasoning.

Charalambous et al. [9] used a similar range in their study on the effects of temperature on mixed mode I/II delamination in carbon-epoxy composite under quasi-static and fatigue loading. Here, temperatures between  $-50^{\circ}\text{C}$  and  $80^{\circ}\text{C}$  are used claiming that they represent operating temperatures, but without information to justify that claim.

Coronado et al. [8] perform test at temperatures between  $-60^{\circ}\text{C}$  and  $90^{\circ}\text{C}$  to research the influence of temperature on carbon-epoxy composites under mode I delamination for static and fatigue loading. With these temperatures, they go just beyond the regular range. This could have been done because they wanted to investigate the outskirts of the nominal temperature range, but this is purely speculation as no clear reasoning for their choices is given.

When reviewing both the temperature conditions that can occur in service and the temperatures used in previous studies [8, 9, 16], any temperature range with extremes close around  $-60^{\circ}\text{C}$  to  $-50^{\circ}\text{C}$  and  $80^{\circ}\text{C}$  to  $90^{\circ}\text{C}$  are considered relevant within the aviation industry.

## 2.3 What influence has temperature on the material properties?

The material that will be used in the experimental phase of this research is M30SC/DT120 cured at  $120^{\circ}\text{C}$  for 90 minutes. This is a carbon fibre reinforced composite with an epoxy matrix. The glass transition temperature,  $T_g$ , for this material with the given curing cycle is  $115^{\circ}\text{C}$  to  $120^{\circ}\text{C}$  [17]. Temperatures close to the  $T_g$  need to be avoided during the tests, as this is where the matrix material becomes viscous and its mechanical properties decrease drastically. With the temperature range as explained in 2.2, this is not a problem.

To understand the effects of temperature on delamination growth, a good understanding of the effect of temperature on the material properties is necessary. At low temperatures, materials are more brittle, while at high temperatures, materials are more ductile. This is also shown in previous studies on temperature effects in fatigue delamination growth [8, 18].

Because of the importance of fibre bridging in fatigue delamination growth, the most important property is the fibre-matrix interaction. To describe this interaction, the strength of the fibre-matrix interface must be assessed. Wang et al. [19] performed experiments to investigate the interfacial shear strength in carbon fibre/epoxy composites at different temperatures between  $23^{\circ}\text{C}$  and  $150^{\circ}\text{C}$ . They concluded that below  $T_g$ , the interfacial shear strength does not show a significant decrease. Koyanagi et al. [20] also studied the temperature dependence of the carbon fibre/epoxy interface. Their experiments were performed at different temperatures between  $25^{\circ}\text{C}$  and  $150^{\circ}\text{C}$ . They concluded that, below  $T_g$  the interface strength is independent of temperature.

## 2.4 How do fracture mechanics apply to fatigue delamination growth in composite laminates?

In this section, the application of fracture mechanics concepts to (fatigue) delamination growth in composite laminates is discussed. First, the concepts of strain energy release rate and stress intensity factor are explained. Then, the importance of similitude parameters in presenting delamination growth data is elaborated on. Finally, the Paris relations are discussed.

### 2.4.1 Strain Energy Release Rate and Stress Intensity Factor

When applying fracture mechanics to fatigue delamination growth in composite laminates, the strain energy release rate (SERR) and the stress intensity factor (SIF) are linked to delamination growth [21]. In order to do that, a good understanding of these parameters is necessary. Both parameters are reviewed and explained in the following paragraphs. After that, the relation between the SERR and SIF is given.

In 1921, Griffith [22] was the first to describe a 'loss' (=release) of strain energy in a developing crack. He concluded that if energy is added to a material and no displacement occurs, this energy is available for crack growth. This crack growth occurs to restore stability in the system. In 1952, Irwin and Kies [23] provided a method to experimentally determine the SERR using the following formula.

$$\frac{dE}{dx} = \frac{dE_s}{Bdy} \quad (2.1)$$

Here,  $\frac{dE}{dx}$  is the strain energy release rate,  $dE_s$  is the change in energy, B is the plate width and dy is the difference in hole/crack length. Over time, Equation 2.1 transformed into a form that is mostly used nowadays. This is depicted by S.M. Kumar [24] in his book on the fundamentals of fracture mechanics:

$$G = -\frac{\Delta\pi}{2B\Delta a} \quad (2.2)$$

Here, G is the SERR,  $\Delta\pi$  is the change in energy, B is the plate width and  $\Delta a$  is the change in crack length and thus the crack growth.

In 1957, Irwin [25] applied Westergaards [26] stress field theory to cracks and was the first to describe an intensity factor around a crack tip. He described this intensity factor to be proportional to the square root of the force tending to cause crack growth [25] and describes the stress field around a crack. At first, the stress intensity factor was only valid for isotropic materials. However, after further research Sih, Paris and Irwin [27] concluded that this could be extended to anisotropic materials.

Now that both the SERR and SIF have been defined, it is worth noting that the SERR and SIF are interrelatable. Their relationship to each other can be given as

$$G = \frac{K^2}{E'} \quad (2.3)$$

For isotropic materials,  $E'$  is equal to the Young's modulus  $E$  under plane stress conditions and is equal to  $\frac{E}{1-\nu^2}$  under plane strain conditions [28]. For anisotropic materials,  $E'$  is given as

$$E' = \frac{(2E_L E_T)^{1/2}}{[(\frac{E_L}{E_T})^{1/2} + (\frac{E_L}{2G_{LT}})^{1/2}]^{1/2}} \quad (2.4)$$

Here,  $E_L$  is the modulus of elasticity along longitudinal direction,  $E_T$  is the modulus of elasticity along tangential direction and  $G_{LT}$  is the shearing modulus of elasticity [29].

### 2.4.2 Similitude parameters

When describing fatigue delamination growth, often scaling laws are used. These scaling laws are functions that aim at empirically correlating similitude parameters to delamination growth. Therefore, it is important to find the similitude parameters that scale best for the given problem. There is still disagreement on the use of similitude parameters.

Both the SERR and the SIF have been used as similitude parameters. When describing fatigue crack growth in metals, the stress intensity factor  $K$  is mostly used [30]. When it comes to composite laminates, the strain energy release rate  $G$  is preferred for characterizing fatigue crack growth [21]. This could well be the only widely supported consensus that exists on the matter. Because the scope of this research is composite laminates, the strain energy release rate  $G$  will be used in the following paragraphs. However, the analogy with the stress intensity factor is easily made.

There is a lot more disagreement on how exactly the role of the similitude parameter is filled in. Some researchers used  $G_{max}$  as similitude parameter [31–33] while others tried using the SERR range  $\Delta G$  [34–36]. Some researchers doubt whether one or the other is an appropriate parameter and tried using combinations of both parameters [37, 38]. In his review on prediction methods for fatigue delamination growth, Pascoe [21] found that many researchers choose  $G_{max}$  or  $\Delta G$  without comparing the two. Intuitively, because of the cyclic nature of fatigue, using the SERR range seems to be more fitting than using the maximum SERR to describe fatigue crack growth. But this turns out not to always be the case. Roderick et al. [39] made a comparison between both parameters and a combination of the two. They discovered that for different material systems, the best parameter for empirical correlations varies, concluding that there is no unique parameter that is always the best similitude parameter.

Rans et al. [40] published a discussion on how the SERR range should be formulated. They concluded that although defining the SERR as  $G_{max} - G_{min}$  is not entirely incorrect, using  $(\sqrt{G_{max}} - \sqrt{G_{min}})^2$  has no dependency on the mean stress and is thus equivalent to the SIF range  $\Delta K$  used in metals. This equivalency can be illustrated when looking at the relation between SIF and SERR given in Equation 2.3. Rans et al. [40] also concluded that using  $(\sqrt{G_{max}} - \sqrt{G_{min}})^2$  is more appropriate for describing fatigue delamination growth compared to  $G_{max}$ .

### 2.4.3 Paris relation

A Paris relation is one type of scaling law using similitude parameters. Other forms of scaling laws are the Hartmann-Schijve equation [41], which is a form of a Nasgrow equation, and several two parameter models like the models described by Hojo [37] and Khan et al. [42]. Although Paris relations are often used to predict delamination growth, they are of a descriptive rather than a predictive nature. In delamination growth studies, Paris relations have often been used to link the strain energy release rate,  $G$ , or the stress intensity factor,  $K$ , to delamination growth [31, 32, 34–37]. The first form of Paris relation, as described by Paris [43, 44], is given as

$$\frac{da}{dN} = C(\Delta K)^m \quad (2.5)$$

Here,  $C$  and  $m$  are curve-fitting parameters. This form of Paris relation is mostly used for metals. For composite laminates, the SIF is often replaced by the SERR. Because of the disagreement on the use of  $G_{max}$  or  $\Delta G$ , or even  $(\sqrt{G_{max}} - \sqrt{G_{min}})^2$  this formula can be generally written as [21]:

$$\frac{da}{dN} = Cf(G)^m \quad (2.6)$$

where  $f(G)$  can be  $G_{max}$  or  $\Delta G$  or  $(\sqrt{G_{max}} - \sqrt{G_{min}})^2$ . Throughout section 2.6, some of the different forms of Paris relations are given. One of the major drawbacks when using Paris relations is the stress ratio effect or R-ratio effect. This effect is still subject of discussion and researchers disagree on its cause and how to use it. For engineering purposes some like to make the effect disappear by cleverly choosing similitude parameters or by using two-parameter models. For research purposes the effect must not disappear. The R-effect will be explained in further detail in Section 2.6.

A Paris relation has, just like other scaling laws, no physical meaning. They are only used to describe relations based on reference data. As a consequence, often constants in scaling laws have units to make the equations sound. Therefor, in the next subsection, a more physical approach to the problem is discussed.

## 2.5 How do energy principles provide a physical approach to fatigue delamination growth in composite laminates?

The use of these similitude parameters in scaling laws only display relationships and data relative to a baseline. In order to have a more absolute way of displaying and comparing data from different specimen and materials, it might be better to go back to the basics as Griffith [22] described them and try to find a description based on energy and physics.

Griffith described a stability criterion [22]. Assuming that the system of the material is a closed system, energy that is released can create an instability in this system which in turn causes crack growth. This cracking releases more energy which causes further crack growth. This continues until equilibrium in the material is restored.

When looking at what happens physically when a material is loaded in fatigue, the following can be concluded. When loading a specimen in fatigue, a cyclic load is introduced. This also means that the addition of energy is cyclic. At  $P_{max}$ , there is a large force applied and thus a lot of energy introduced into the specimen. However, at  $P_{min}$  there is still energy present in the specimen. This means that damage can still occur at the minimum load. This is one of the conclusions Motta [45] drew from his research. He used the acoustic emission technique to determine the strain energy dissipation in fatigue and to create a physical understanding of fatigue delamination growth in fibre reinforced polymers. With this technique, he observed a threshold for damage propagation. All loads above this threshold enable damage propagation. This means that if the lower limit of the fatigue load is above this threshold, damage is created in the entire fatigue cycle. This threshold value was also previously reported by Pascoe et al. [46]. Pascoe used a fracture mechanics based approach, while Motta based his research on energy principles. An important note to this is that above this threshold damage propagation does not occur by itself. Energy will still need to be introduced in the material in the form of the fatigue load to have damage propagation.

This threshold value can be explained using the resistance of the material. If the driving force is smaller than the resistance, i.e. below the threshold, there is no crack growth. However, when the driving force is larger than the resistance, i.e. above the threshold, the extra energy is dissipated in the form of crack growth. This can be seen in how Jones et al. [41] interpreted the work of Hartman and Schijve [47]. From this, they deduced the 'Hartman-Schijve equation'

$$\frac{da}{dN} = D \left( \frac{\Delta\sqrt{G_I} - \Delta\sqrt{G_{Ith}}}{\sqrt{1 - \frac{\sqrt{G_{Imax}}}{\sqrt{G_{Icy}}}}} \right)^\beta \quad (2.7)$$

Here, there is a  $G_{max}$  term in the denominator. This term increases with increasing resistance.  $\beta$  and  $D$  are constants,  $\Delta\sqrt{G_{Ith}}$  is the mode I delamination threshold and  $\sqrt{G_{Icy}}$  is the mode I delamination fracture toughness [41].

When using energy principles to explain a fatigue cycle, the above mentioned concepts of dissipated energy and applied energy become clear. Alderliesten [48] formulated a single cycle as:

$$U_0 + U_\uparrow \rightarrow U_0^* + U_\downarrow + U_a + U_{pl} \quad (2.8)$$

Here,  $U_0$  is the monotonic strain energy available at minimum load,  $U_a$  is the energy dissipated through damage growth,  $U_{pl}$  is the plastically dissipated energy and  $U_0^*$  is the monotonic strain energy available at minimum load for the next cycle.  $U_\uparrow$  and  $U_\downarrow$  represent the elastic cyclic work, the work applied to the specimen during loading and the work applied by the specimen during unloading respectively [48, 49]. The applied work per cycle can be calculated using

$$U = 0.5P_{max,N}\delta_{max,N} \quad (2.9)$$

where  $P_{max,N}$  and  $\delta_{max,N}$  are the maximum force and displacement in the  $N^{th}$  cycle respectively [2]. Equation 2.9 is valid when the P- $\delta$  graph goes through the origin. When the applied work per cycle is plotted with respect to the number of cycles, the slope of this  $dU/dN$  curve is the strain energy release per cycle. This strain energy release per cycle can be written as the product of the crack growth per cycle  $da/dN$  and the energy dissipated per area of crack created, which is the resistance to crack growth,  $dU/da$  [48, 49]. This can be written as:

$$\frac{dU}{dN} = \frac{dU}{da} \frac{da}{dN} \quad (2.10)$$

With this information, the energy dissipated per area of crack created can be displayed by plotting  $dU/dN$  vs.  $da/dN$ . This plot represents the resistance in fatigue delamination growth.

## 2.6 What are the critical parameters for fatigue delamination growth at room temperature?

In this section, two important parameters for fatigue delamination at room temperature are explained. First, the stress ratio effect is elaborated on and after that, the fibre bridging phenomenon is discussed.

### 2.6.1 Stress ratio effect

The stress ratio,  $R$ , is the ratio of the minimum stress to the maximum stress in a cycle [50]. Simply said, the stress ratio effect is that a higher stress ratio causes an increase in crack growth rate for a given  $\Delta G$  or  $\Delta K$ . However, there is a lot of disagreement among researchers on the stress ratio effect and there is a lot more to it than just this simple explanation.

Researchers have found very different results dependent on which similitude parameter was used in paris type relations. Mall [32], Hojo [37] and Shahverdi [33] all came to the conclusion that when using  $G_{max}$  as similitude parameter, the stress ratio effect was clearly visible. When using  $\Delta G$  however, the stress ratio effect became ambiguous. This lead Mall to the conclusion that  $\Delta G$  is the driving parameter for cyclic debonding in adhesively bonded joints [32]. He came to this conclusion because the absence of a stress ratio effect was a good thing in his opinion as this brought all curves of specimens tested under different stress ratios together. This observation was also made by Khan et al. [51]. When using  $(\sqrt{G_{max}} - \sqrt{G_{min}})^2$  however, the R-ratio effect became clearly visible. Therefore, they concluded,  $(\sqrt{G_{max}} - \sqrt{G_{min}})^2$  is a better similitude parameter than  $\Delta G$  for the purpose of researching the R-ratio effect.

Khan also pointed out that, ideally, in linear elastic fracture mechanics there should not be an R-ratio effect. This is because the R-ratio effect likely is attributed to non-linear effects such as the presence of broken fibres, fibre pullout and crack closure due to asperities [51].

A similar physical explanation is provided by Yao [2]. He found that with the increase of the stress ratio, fatigue resistance increased. This is due to a rougher fracture surface at high stress ratio, which can be said is similar to the observations Khan made about the broken fibres, fibre pullout and asperities.

From acoustic emission experiments carried out by Motta [45], he observed that not only the stress ratio is important, but also the values of  $P_{max}$  and  $P_{min}$  are of significance. He discovered a threshold level of energy that needs to be overcome to enable damage propagation and thus crack growth. When  $P_{max}$  and  $P_{min}$  are both above this threshold, damage can

also develop during unloading. This leads to wonder if the stress ratio effect might not be caused by the stress ratio but by high absolute loads. Amaral [49] takes it one step further and states that *"the term "stress ratio effect" is found to be inappropriate and misleading in case of representing delamination resistance"* (Amaral, [49] p.88). In his PhD research, Amaral concluded that the shift observed in Paris type curves has no connection to physical mechanisms that occur during fracture and he attributes the R-ratio effect purely to how the data is presented. He therefore suggests that one should refer to *"changes in delamination resistance due to loading parameters"* (Amaral, [49] P.87) instead of the R-ratio effect. This also puts the findings of Khan and Yao in another perspective. The physical observations they made and attributed to the R-ratio effect, might in fact be caused by the high absolute value of the stress applied, and not necessarily by the stress ratio as such. It is very hard to investigate whether one or the other caused the observed effects, but it can be said that taking into account both stress ratio and stress values could provide a broader view and more useful information. Researchers tried to achieve this by using models with two parameters.

The stress ratio effect is very dependent on the used similitude parameter, which is inherent to one parameter models, as mentioned previously. This, combined with the knowledge that one parameter does not provide enough information to completely describe fatigue loading [36,37], researchers turned to two parameter models. These models mostly use both  $G_{max}$  and  $\Delta G$ , or  $K_{max}$  and  $\Delta K$ . An example of such a two parameter model, a model in analogy with the Paris relation as proposed by Hojo, is given as

$$\frac{da}{dN} = c\Delta K^{(1-\gamma)}K_{max}^{\gamma n} \quad (2.11)$$

Here,  $\gamma$  is an empirical material parameter that indicates the significance of  $K_{max}$ . Many different two-parameter models, using different relations between the parameters, have been used in the past [36,37,42,52]. Using these two-parameter models, the stress ratio effect disappears. This makes perfect sense as the two-parameters are chosen as such that all curves come together. These models, however, are still empirical models and thus have no physical meaning. They are simply a way to display the data in a manner that is useful for the study in which they are used. An engineer researching a practical application may want the stress ratio effect to disappear and use a two-parameter model to do so, while a scientist might want to study the effect and therefore use a single parameter model that clearly displays it.

### **2.6.2 fibre bridging**

Fibre bridging is a phenomenon in which fibres in composite materials store elastic energy across a crack or delamination, increasing the fracture toughness and thus slowing down the crack or delamination rate. It is often called a shielding mechanism, because it 'protects' the material against crack growth by absorbing a lot of the introduced energy [2,53]. Fibre bridging is mostly attributed to fibre nesting and weak fibre-matrix interfaces [54]. Nesting is a phenomenon in which the fibres migrate between layers during the curing cycle. This obscures the clear delamination plane between the layers. Nesting is common in unidirectional laminates because when all fibres are in the same direction, migrating between layers is easier.

Another cause for fibre bridging was investigated by Bradley and Cohen [55]. They observed that in tougher resin matrix composites, the crack tip yield zone can extend to several plies above and below the delamination layer. This leads to more delamination and debonding in the surrounding interfaces, after which these fibres will cause the same effects as bridged fibres in the delamination plane. This was also confirmed by research done by Khan et al. [56].

When fibre bridging occurs, the crack growth rate is decreased significantly. This is because the bridging fibres increase the fracture toughness of the material by absorbing a lot of the applied load as strain energy [2, 57]. In fatigue loading, the bridging fibres store and release that strain energy during a loading cycle [58]. When researching the stress ratio effect, Khan developed a fracture mechanics based model for fatigue delamination growth [56]. He stated that fibre bridging had no influence on the stress ratio and thus a single resistance curve could be used to determine fatigue delamination growth with or without fibre bridging. Later, Yao [2] claimed that this conclusion was premature. In his study, Yao ran his tests until a higher level of bridging compared to Khan, and he concluded that it is impossible to use only one resistance curve to determine fatigue delamination growth with fibre bridging. Yao [2, 59] proposed an alternate form of the Paris relation. By correlating empirical parameters  $C$  and  $n$  to the crack extension, a single Paris relation can be used to accurately describe fatigue delamination growth with fibre bridging. This form of the Paris relation is given as

$$\frac{da}{dN} = C (a - a_0, R) \Delta G^{n(a-a_0, R)} \quad (2.12)$$

where  $a - a_0$  is the crack extension.

When looking at fibre bridging from an energy perspective, it can be said that fibre bridging has only a small contribution to the strain energy release rate. This is because all the energy that a bridging fibre absorbs during loading, it releases again during the unloading phase of the same cycle [2].

To describe fibre bridging, two methods can be used. The first method is using resistance curves or R-curves. In a resistance curve, the relation between crack growth resistance and crack growth is displayed [60]. The second method is using a so called bridging law, which is the relation between local crack opening  $\delta$  and local bridging stress  $\sigma$  [60, 61]. When it comes to small scale bridging, when the fibre bridging area is much smaller than the smallest specimen dimension, both methods can be considered to represent a material property. However, in large scale fibre bridging, when the fibre bridging area is equal to or exceeds the smallest specimen dimension, the R-curve is no longer a material property because it is geometry dependent [60].

As explained in Section 2.5, a resistance curve can be generated by making a plot of the crack growth per cycle  $da/dN$  versus the strain energy release per cycle  $dU/dN$ . Using this relationship, the energy that is dissipated per area of crack created, which is the resistance to crack growth, can be depicted [48, 49]. As mentioned before, Yao [2] observed that bridging fibres have little influence on the strain energy release rate because the energy absorbed during loading is released during unloading of the same fatigue cycle. However, he found that when a bridging fibre failed or there was fibre pullout, this energy was released permanently.

Bridging laws attempt to describe the effects of fibre bridging using the stress distribution in the bridging area by finding an expression for the bridging stress  $\sigma$  as function of the crack opening displacement and the material resistance. A general form of bridging law, determined with the J-integral method, is given as

$$\sigma(\delta^*) = \frac{\partial G_R}{\partial \delta^*} \quad (2.13)$$

Here,  $G_R$  is the material resistance, obtained from the R-curve, and  $\delta^*$  is end-opening of the bridging zone [60].  $\sigma(\delta^*)$  obtained from the bridging law can be considered a material property as it is not dependent on specimen geometry and therefore is a universal way of describing the effect of fibre bridging. Jacobsen et al. [61] measured both the R-curve and bridging law. From that bridging law, they then calculated a prediction for the R-curve to compare to the measured R-curve. Their conclusion was that these two curves were very similar. This is a logical conclusion to make since the simulated R-curve is based on the bridging law which, in turn, is based on data from the measured R-curve.

As mentioned before, the bridging law is considered a material property independent of geometry and thus more universal compared to the R-curve. For the purpose of this research the data collected from testing is all from specimens of the same geometry. Therefore, using a bridging law has no advantage over using energy principles based resistance curves. In this research, the latter will be used to describe fibre bridging. This is also the case for the data collected by Yao [2], which will be used for comparison.

As Johnson [54] already discussed, there are two ways to look at fibre bridging. Firstly, the high fracture toughness resulting from fibre bridging can be useful in applications where high fracture toughness is needed. Secondly, fibre bridging is undesirably when trying to determine the fracture toughness of the composite laminate because it has such a large effect on the values. Basically, when encountering fibre bridging, one can ask one of two questions: How can I use it? Or how can I get rid of it?

Because fibre bridging drastically increases the fracture toughness, it can potentially be very useful. However, counting on fibre bridging for strength is also dangerous. Firstly, bridged fibres can break or pull-out. When this happens, there is a chance that this leads to a 'zip-effect' and cause the entire (part of the) structure to fail. Secondly, when fibre bridging does not occur in the structure, the material has to take more load than it can in reality. As fibre bridging is unlikely to occur naturally in structures, it mostly happens in a controlled laboratory environment [53], it is quite dangerous to rely on bridged fibres to keep a structure from failing.

In order to have a potential application in the future, much more research is needed to fully understand the phenomenon.

## 2.7 What is the effect of temperature on fatigue delamination growth?

When it comes to temperature effects on mode I fatigue delamination growth, not a lot of publications can be found. It is a relatively new area of research. a couple of studies have been found and their conclusions will be given here in order to have an idea as to what results can be expected from the experimental campaign.

In their study of a fibre bridging model for fatigue delamination, Gregory and Spearing [62] performed DCB tests in a temperature range between 24°C and 149°C. They developed a model to separate SERR contributions of fibre bridging and propagation of the crack in resin. After applying this model to their test data, higher crack propagation rates were observed at higher temperatures for a given maximum applied SERR.

Coronado et al. [8] performed tests in a temperature range from -60°C to 90°C. They discovered that during initiation of fatigue delamination, the maximum energy required to initiate a crack increased with increasing temperature, due to matrix ductility. For temperatures between 0°C and 90°C, a constant delamination growth rate  $da/dN$  was observed in fatigue propagation of the crack. For the temperatures below 0°C, the crack growth rate was significantly higher, decreasing as the crack progressed [8, 18]. This indicates brittle behaviour of the matrix. When comparing quasi-static and fatigue tests, it was shown that the influence of temperature was larger in fatigue test, possibly due to the longer test duration. Quasi-static tests showed the best performance at room temperature, while for fatigue tests, the material had a greater resistance to delamination at 90°C. Later, in another study, Coronado et al. [18] concluded that decreasing temperatures below 0°C had a higher crack growth rate, which means the material has a lower resistance against fatigue crack growth.

Sjörge and Asp [63] performed Mode I tests under static and fatigue loading at room temperature and at 100°C. They observed that for static loading, the critical SERR only slightly decreased. Although they don't describe it in their report, from their results it can be seen that the SERR threshold for fatigue loading at 100°C was 50% lower compared to tests at 20°C.

Because it was very difficult to find studies about the effect of temperature on carbon fibre/epoxy laminates under fatigue loading, next some studies on the effect of temperature on glass/fibre epoxy laminates, fibre metal laminates and epoxy bonded composite joints will be discussed. These materials are not perfectly comparable to the material that will be used in the experimental phase of this research, but they can provide insight in what might happen and help towards making an estimated guess.

Chan and Wang [64] investigated glass fibre/epoxy laminates. They observed that at -55°C, specimens showed the lowest fracture toughness. The effect of temperature on growth rate was less clear from their study.

In fibre metal laminates (FML), Rans et al. [65] concluded that resistance to delamination growth to decreased for both low (-40°C) and elevated (70°C) temperatures. At elevated temperature, the decrease was smaller compared to low temperature.

In Bonded joints, Ashcroft et al. [66, 67] observed the lowest fatigue resistance at the highest test temperature (90°C). Also for low temperatures (-50°C), there was a higher fatigue crack growth [67].

To summarize, it can be said that the different studies produced somewhat different results. When it comes to experiments performed on carbon fibre/epoxy composites, both Gregory and Spearing [62] and Sjörgen and Asp [63] observed higher crack propagation rates with increasing temperatures. To the contrary, Coronado et al. [8,18] discovered that more energy was needed to initiate a delamination, and after initiation delamination growth rates were constant. At subzero temperatures, Coronado et al. [8,18] observed that the resistance decreases with temperature.

The studies on different materials/situations, which can provide a general direction of expectations, had some different outcomes. This is not very strange as they all researched different things. Rans et al. [40] concluded that delamination growth decreases for both low and elevated temperatures in FML. Ashcroft et al. [66,67] observed lower fatigue resistance for both low and elevated temperatures. This is similar to what Gregory and Spearing [62] and Sjörgen and Asp [63] observed. Chan and Wang [64] could not make any conclusions on crack growth rate, but for subzero temperatures, they observed lower fracture toughness with decreasing temperature.

When analyzing the data from the experimental phase of this research project, it will be interesting to compare to these studies and see what the outcomes will be.



---

## Chapter 3

---

# Research Questions

After studying the literature in the field of delamination growth in composite laminates, research questions for the experimental work of this thesis project were formulated. These research questions were formulated as such that when answered, the objective of the master thesis research is reached. For the given topic of investigating the effect of ambient temperature on fatigue delamination growth in composite laminates, there is one main research question:

*What is the effect of ambient temperature on fatigue delamination growth in composite laminates?*

This question is very comprehensive and thus, it is split up into three sub-questions that answer specific parts of the main question. These sub-questions are the following.

1. What is the influence of ambient temperature on fibre bridging under fatigue loads in composite laminates?
2. What is the influence of ambient temperature on the quasi-static and fatigue delamination resistance (curve)?
3. Does the stress ratio effect on fatigue delamination growth change with temperature?

The methodology that will be used to answer these questions is explained in Chapter 4.



---

# Chapter 4

---

## Methodology

In this chapter, the methodology that was used to answer the research questions is explained. First, the material and specimen manufacturing is discussed. then, the experimental campaign and test-setup are discussed. After that, the methods used for data analysis are elaborated on. finally, data representation is touched upon.

### 4.1 Material and Specimen Manufacturing

This research project limited itself to unidirectional specimens. These consist of 32 plies in a  $[0_{16}/0_{16}]$  layup with a  $15\mu\text{m}$  Teflon insert at the midplane. The Teflon insert is 60mm long in the fibre direction and was used to create a weak spot at the midplane to ensure delamination initiates at the same position in every specimen. The prepreg material used for manufacturing the DCB specimens necessary for performing the experiments was M30SC/DT120, a carbon fibre epoxy supplied by Delta-Tech S.p.a. Italy. The elastic properties of this prepreg are given in Table 4.1

**Table 4.1:** Elastic properties of the prepreg M30SC/DT120 [2]

Longitudinal elastic modulus $E_{11}$ [GPa]	155
Transverse elastic modulus $E_{22}$ [GPa]	7.8
In plane Poisson ratio $\nu_{12}$	0.27
In plane shear modulus $G_{12}$ [GPa]	5.5

This material was manufactured into a total of 2 laminates of 250mm in fibre direction with a width of 600mm using the process of hand layup. These laminates were cured in an autoclave at  $120^{\circ}\text{C}$  and a pressure of 6 bars for 90 minutes. The curing procedure is shown in Figure 4.1.

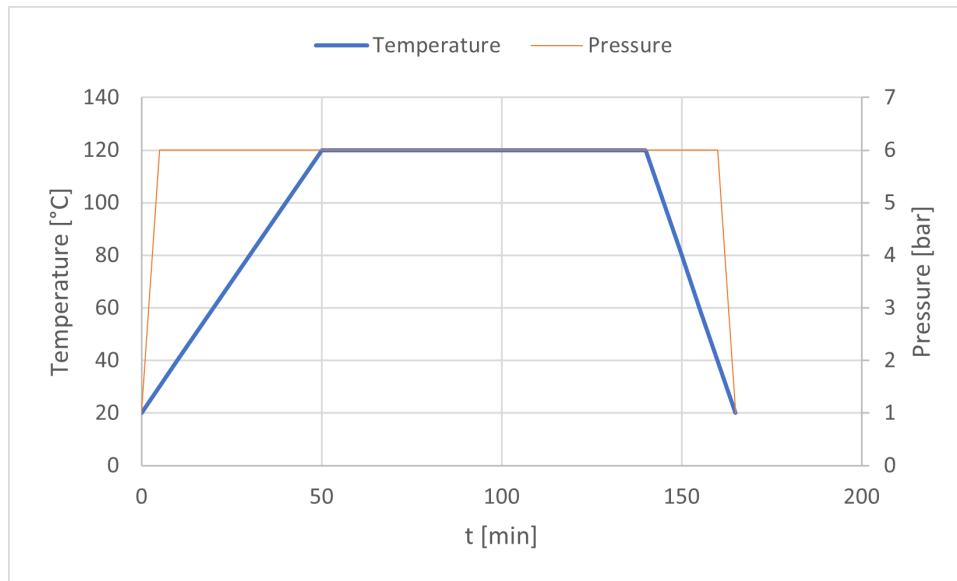


**Figure 4.1:** Autoclave curing procedure

After curing, the laminates were C-scanned to look for imperfections and finally were cut into 200x25mm specimens. These specimens were outfitted with load introduction blocks and a mm-grid for delamination length measurement. Additionally, one side of the specimens was painted white for a better visibility of the delamination growth. A picture of the specimen with insert and load introduction blocks is shown in Figure 4.2.

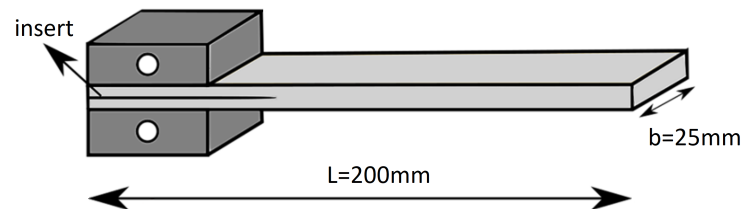


**Figure 4.2:** DCB specimen; Figure taken from [1] and modified to personal need

## 4.2 Experimental Campaign and Test Setup

First, the development of the experimental campaign and how this relates to the research questions is explained after which the test setup necessary to conduct the experimental campaign is shown.

### 4.2.1 Experimental Campaign

In order to gather the data needed for answering the research questions, double cantilever beam (DCB) tests were performed. The experimental campaign for this research project was split into two parts: quasi-static delamination tests and fatigue delamination tests. All tests that were performed are given in Table 4.2 and Table 4.3 for the quasi-static and fatigue experiments respectively. Quasi-static tests were performed according to ASTM D5528 [68]. Fatigue tests were performed according to the test protocol by Alderliesten and Brunner [69]. First, some general aspects of the experiments are discussed. After that, in Subsection 4.2.2 and Subsection 4.2.3 specific points for each type of test are discussed.

The first couple of tests were performed at room temperature. This was done to be able to get acquainted with the test procedure and be able to verify against the test results obtained by Yao [2]. If the results from these tests are similar to results obtained by Yao, it can be considered valid to compare tests at elevated and low temperatures to Yao's RT tests for discussing temperature effects. This means it can be assumed that the test procedures have a good repeatability.

All tests were conducted on different temperatures between  $-50^{\circ}\text{C}$  and  $80^{\circ}\text{C}$ , a range that has proven to cover the operational temperatures of composites in aircraft as was explained in Section 2.2. The temperatures at which tests were performed are  $-40^{\circ}\text{C}$ , Room temperature,  $50^{\circ}\text{C}$  and  $80^{\circ}\text{C}$ . These temperatures were chosen because they cover both low, medium and elevated temperatures. Although originally  $-50^{\circ}\text{C}$  was chosen, instead of  $-40^{\circ}\text{C}$ , but with the limitations of the temperature chamber available it proved too difficult to provide a stable  $-50^{\circ}\text{C}$  temperature for the duration of a test. Using a thermocouple, the temperature inside the temperature chamber was checked to ensure a stable temperature throughout the test.

### 4.2.2 Quasi-static Test Campaign

Quasi-static tests were performed to generate resistance-curves to compare to the fatigue data later on. During the quasi-static test campaign, the test machine automatically recorded the force and displacement. Using a camera, at time intervals of 5s, an image of the specimen was recorded to measure the delamination length and observe the fibre bridging phenomenon. The force, displacement and delamination length data were coupled using two methods.

Using the first method, the force and displacement data are recorded by the test machine and sent to the computer that controls the camera. At every image that is taken, the data is stored simultaneously. To send the force and displacement data from one computer to another, the data is converted to voltages and converted back to force and displacement after the data transfer. These conversions cause inaccuracies in the data. When plotted, this is shown as data scatter. This method of data collection was used in every quasi-static test performed except one.

The second method was used for one quasi-static test at room temperature, and is the same method of data collection that Yao used in his PhD thesis [2]. This method makes use of two cameras. One to record the images of the specimen for delamination length calculation and a second camera that records images of the computer screen that is controlling the test machine. Doing so, the force and displacement data is logged directly from the test machine and thus no data scatter caused by data transfer is present. The downside of this method is that it requires more manual labour as the force and displacement data has to be read of the images and inputted in an excel file by hand. This method used by Yao was duplicated to have a better understanding of how test and data acquisition methods can influence the results of a test. The data collected during the quasi-static tests aided in answering the second research question.

In Table 4.2, a summary of the quasi-static tests can be found. As seen from the table, each test case was repeated three times.

**Table 4.2:** Quasi-static test campaign

Loading	Laminate layup	Temperatures	Data recording	related to research question	Number of specimens
Quasi-static	UD	-40°C	Delamination length,	2	3
		RT	Force,		3
		50°C	Displacement,		3
		80°C	Temperature		3

### 4.2.3 Fatigue Test Campaign

To capture the stress ratio effect, tests were performed at two different stress ratios,  $R=0.1$  and  $R=0.5$ , like Yao [2] performed in his PhD research.

During the fatigue tests, the test machine automatically recorded the force, displacement and number of cycles. Using a camera, an image of the specimen was recorded at maximum displacement in the cycle to measure the crack length and observe the fibre bridging phenomenon. The intervals at which images were taken are 100 cycles for the first 5000 cycles, 500 cycles between 5000 and 20000 cycles and 1000 cycles above 20000 cycles as prescribed in the test protocol [69]. During fatigue testing, the coupling of the force, displacement, cycle number and delamination length data was much easier. Because both the recording of the force and displacement data and the images was cycle number based, it was possible to directly couple all the data.

In addition to data recordings necessary to perform this research project, acoustic emissions data was also recorded during some of the tests. This data was not used in this research project, but since fatigue delamination experiments at temperatures different from room temperature are not often performed, it was decided to record the acoustic emissions data for other people to use.

To answer research question one, the specimens were repeatedly tested to obtain test results with different amounts of fibre bridging. Then, data for the different amounts of fibre bridging that occurred were compared to each other to see the influence of fibre bridging on fatigue delamination growth at every temperature and the possible change of this effect with temperature. The output data of the fatigue tests was compared for the different temperatures together with the data collected from the quasi-static tests to answer research question two. Because tests were performed at two stress ratios, the third research question concerning the stress ratio effect could also be answered.

A summary of the fatigue tests is given in Table 4.3. When the data from these tests was processed and analysed to answer the research questions, the combined results from this analysis were combined to formulate an answer to the main question. As can be seen from the table, each test case was repeated two times.

**Table 4.3:** Fatigue test campaign

Loading	Laminate layup	Temperatures	R-ratio	Data recording	related to research question	Number of specimens
Fatigue	UD	-40°C	0.1	Delamination length, Force, nr. of cycles, Displacement, Acoustic emissions, Temperature	1, 2, 3	2
			0.5		3	2
		RT	0.1		1, 2, 3	2
			0.5		3	2
		50°C	0.1		1, 2, 3	2
			0.5		3	2
		80°C	0.1		1, 2, 3	2
			0.5		3	2

#### 4.2.4 List of Experiments

In Appendix A, a list of all experiments that were conducted is given. All test ID and specimen ID numbers are given together with the corresponding load case, fibre direction, temperature and stress ratio if applicable.

#### 4.2.5 Test Setup

For performing both quasi-static and fatigue tests the MTS 15kN fatigue machine in the Aerospace Structures and Materials Laboratory at Delft University of Technology was used. To perform DCB tests, the specimen with two load introduction blocks was attached to the fatigue machine by pinned connections at the top and bottom load introduction block.

The fatigue machines load cell and the specimen connected to it were placed into a chamber made of insulating material. This was connected via two tubes to a temperature chamber that generated the required temperature. For cooling down to sub-zero temperatures, liquid nitrogen was used. The front of the insulation chamber has a window in front of which a camera and light source were placed. The window is detachable for easy access to the

specimen. The acoustic emissions sensor was attached on top of the specimen. In the insulation chamber just above the specimen, a thermocouple was installed. This measured the temperature inside the chamber to ensure there was a stable temperature throughout the test. If not, this might influence the test. To keep the window from freezing over during sub-zero testing, a heat gun was added to act as anti-frost. The complete test setup is shown in Figure 4.3. A detail depicting the specimen in the fatigue machine can be seen in Figure 4.4

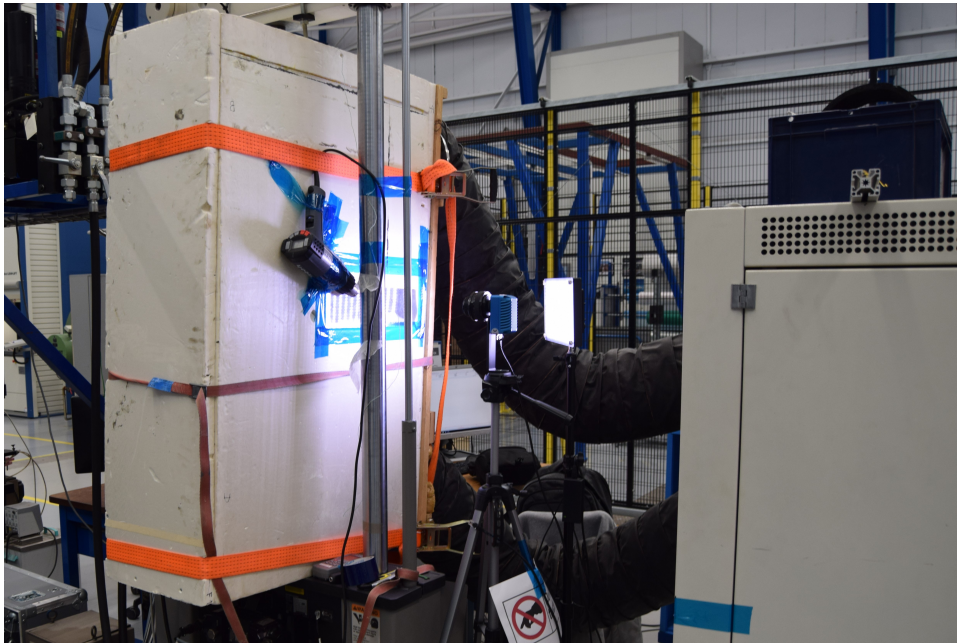


**Figure 4.3:** experimental setup for DCB testing at different temperatures



**Figure 4.4:** detail from experimental setup for DCB testing at different temperatures depicting the test specimen attached to the fatigue machine

### 4.3 Data Analysis

First, the raw data needed to be converted from the machine output data into a workable format. Using a custom python program, the machine output data was converted into an excel file ready for data analysis. The delamination lengths that were captured using images needed to be added to this excel file. The images were processed using a software called 'imageJ'. With the mm-grid added to the specimen for reference, the crack lengths were measured. Since both delamination length images and force and displacement data were measured on a cycle based interval, during fatigue testing, coupling the data was straightforward.

For the quasi-static data, coupling the data was a bit more difficult. As previously explained, two methods for data collection and processing were used. The first method collects all data (delamination length images, force and displacement) on the computer controlling the camera so the force and displacement data were coupled with the delamination length. However, due to the data transfer as a voltage from one computer to another, there was too much data in the force and displacement data to be able to accurately perform calculations and draw graphs. Therefore, a least squares fit of the force and displacement was made. This least squares fit was then compared to the force and displacement data directly from the test machine, which has not been corrupted by converting to a voltage. If the least squares was found to be a good fit compared to the actual data, the corresponding data points from the actual measurements could be used as they were coupled to the delamination length images through the least squares fit.

Since in this research both fracture mechanics and energy principles were used to generate resistance curves and zero bridging curves, both the strain energy release rate (G) and the strain energy release per cycle (dU/dN) needed to be calculated.

The SERR was calculated using the modified compliance calibration method as explained in ASTM D5528 [68] using the equation:

$$G_I = \frac{3P^2C^{2/3}}{2A_1bh} \quad (4.1)$$

Here, P is the load, C is the compliance of the DCB specimen,  $A_1$  is the slope of the curve where  $a/h$  is plotted against  $C^{1/3}$ , b is the specimen width and h is the specimen thickness. In addition to the SERR, also the delamination growth per cycle or fatigue delamination growth rate  $da/dN$  needed to be calculated. According to ASTM E647 [68], this was done using the 7-point incremental polynomial method. The results can then be depicted in a graph of SERR range  $\Delta G$  vs delamination growth per cycle  $da/dN$  where  $\Delta G$  is given as  $(\sqrt{G_{max}} - \sqrt{G_{min}})^2$ .

The energy based approach starts with applied work U. This was calculated from the raw data as follows:

$$U = 0.5P_{N,max}\delta_{N,max} \quad (4.2)$$

Where,  $P_{N,max}$  and  $\delta_{N,max}$  are respectively the maximum force and displacement of the  $N^{th}$  cycle. Subsequently, The derivative of the applied work w.r.t. cycle number dU/dN was calculated in a similar way as  $da/dN$  was explained earlier. The same 7-point incremental

polynomial method was used. Using these energy principles,  $dU/dN$  vs.  $da/dN$  was plotted. This plot shows the energy dissipated per area of crack created and represents the resistance in fatigue delamination growth.

Using these processing and analysis techniques, the data necessary for depicting the results and answering the research questions was obtained. The results from this analysis are given in the next chapter.

## 4.4 Data Representation

During the experimental campaign of this research project, data was recorded with an interval of 5 seconds during the quasi static tests and with an interval of 100 for the first 5000 cycles, an interval of 500 between 5000 and 20000 cycles and an interval of 1000 beyond 20000 cycles during the fatigue tests. For fatigue tests, as a precaution to not have hard to read graphs, for cycles above 20 000, data points were analyzed with an interval of 5000 cycles. This is still in line with the aforementioned test protocol [69]. In Figure 4.5, a  $\Delta G$  vs  $da/dN$  graph of six experiments on a specimen at  $R = 0.1$  and  $T = 50^\circ\text{C}$  is shown. Please note that in the remainder of the report,  $(\sqrt{G_{max}} - \sqrt{G_{min}})^2$  is written as  $\Delta G$  for short.

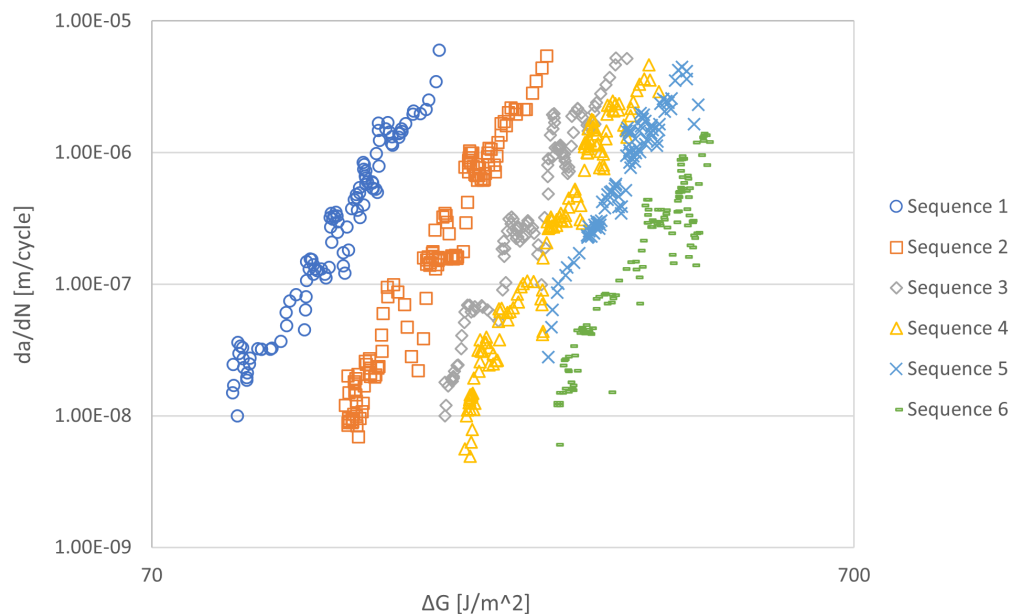


**Figure 4.5:**  $\Delta G$  vs  $da/dN$  graph of six tests on a specimen at  $R = 0.1$  and  $T = 50^\circ\text{C}$

From Figure 4.5 it becomes clear that there is too much data in the graph to see clear lines, especially when the curves for the different test sequences get closer together. To increase graph readability it was decided to reduce the number of datapoints included. A comparison of different amounts of datapoints was made to make sure that the graphs were both easy to read and would still be a good representation of the total picture. As can be seen in Figure 4.6, it was found that using one in every five datapoints provides a good representation of the total picture. Comparing Figure 4.7 to Figure 4.5, it can be seen that graph readability has significantly increased.

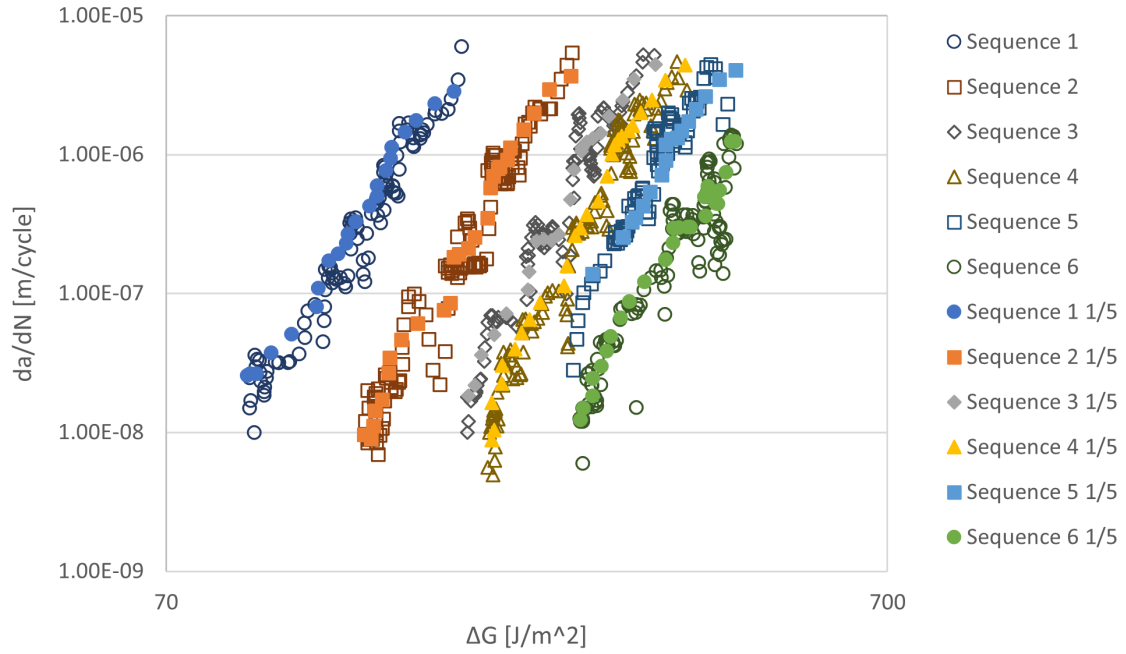


**Figure 4.6:**  $\Delta G$  vs  $da/dN$  graph of six tests on a specimen at  $R = 0.1$  and  $T = 50^\circ\text{C}$  comparing different amounts of data points

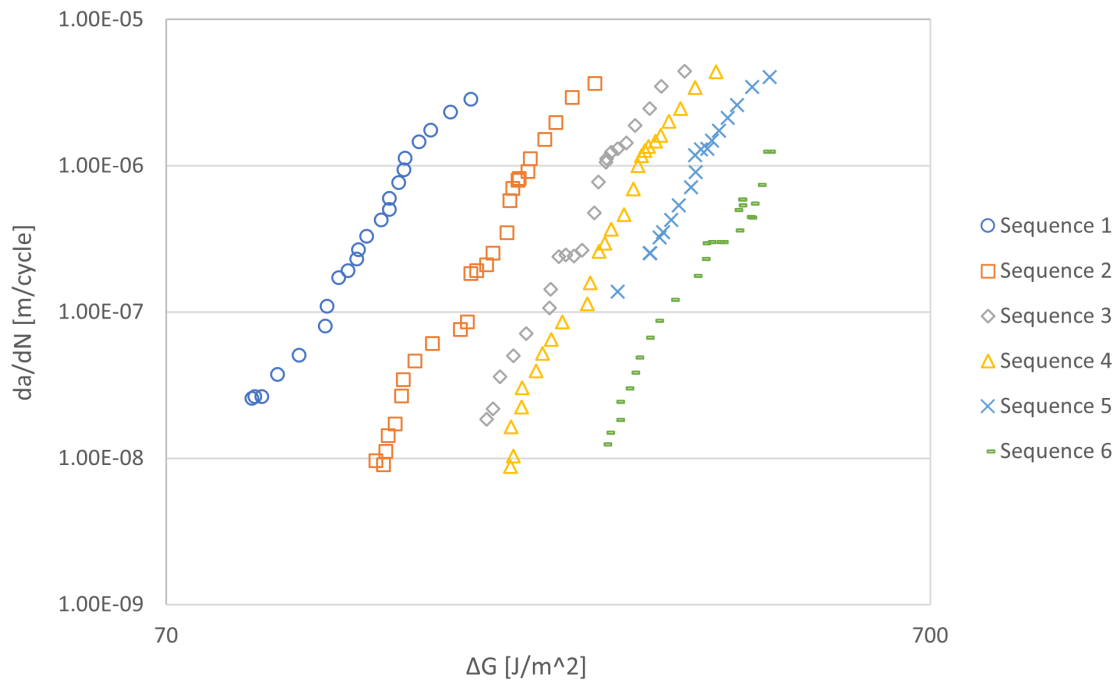


**Figure 4.7:**  $\Delta G$  vs  $da/dN$  graph of six tests on a specimen at  $R = 0.1$  and  $T = 50^\circ\text{C}$  using one in every five datapoints



---

# Chapter 5

---

## Results

In this chapter, the results of the experimental campaign are given. First, the room temperature results are given. Then, the temperature influence on quasi-static and fatigue delamination resistance is touched upon. After that, the influence of ambient temperature on fibre bridging is elaborated on. Finally, the temperature influence on the stress ratio effect is shown.

### 5.1 Room Temperature Data

The data gathered during room temperature tests is analyzed in three separate parts. First, the quasi-static data is touched upon. After that, the fatigue data at  $R=0.1$  is explained and finally, the fatigue data at  $R=0.5$  is elaborated on. Later on, in Chapter 6, the room temperature results are compared to results obtained by Yao in his PhD thesis [2].

#### 5.1.1 Quasi-static Data

In Figure 5.1, force-displacement results for all three quasi-static tests that were performed at room temperature is given. As previously discussed in Chapter 4, two methods for data collection were used. For tests QS\_UD\_RT\_01 and QS\_UD\_RT\_02 the same method was used as for tests at different temperatures, namely storing the force and displacement data together with the images taken of the delamination length. For test QS\_UD\_RT\_03, the method used by Yao [2] was used where he took images of the delamination length and force and displacement gauges simultaneously to ensure the correct force and displacement data was coupled to the delamination length data. Both methods yield almost identical force-displacement data.

Figure 5.2 shows the resistance curves for tests QS\_UD\_RT\_02 and QS\_UD\_RT\_03. The data of test QS\_UD\_RT\_01 was too corrupted by data scatter to produce results. Both resistance curves are very similar to each other. The SERR shows a linear increase with increasing delamination length until about 80mm of delamination length. After this point, a plateau is reached. This plateau in SERR value indicates that fibre bridging is fully developed.

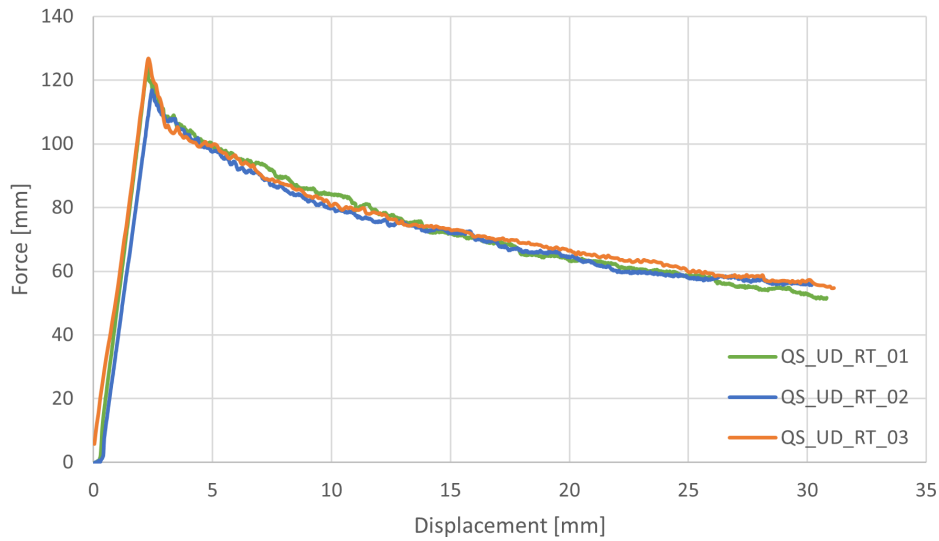


**Figure 5.1:** Force-displacement graph for quasi-static tests at room temperature

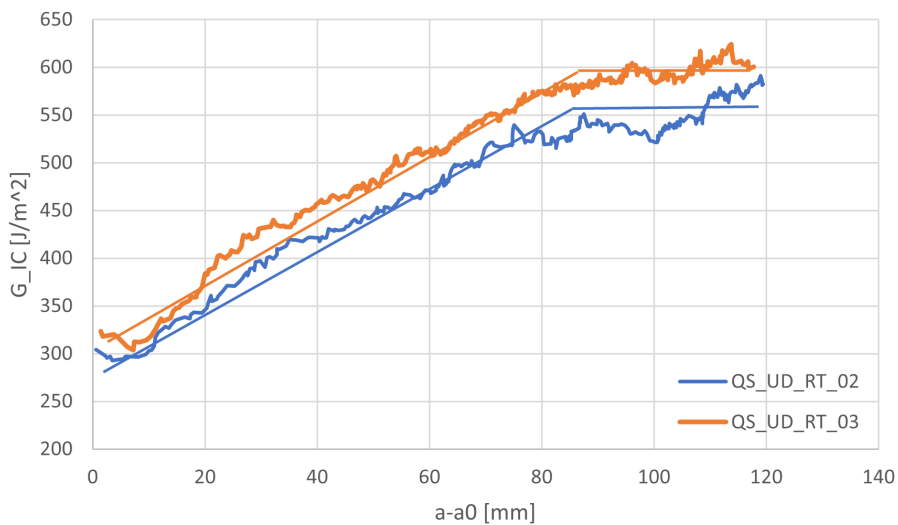


**Figure 5.2:** resistance curves for quasi-static tests at room temperature

### 5.1.2 Fatigue Data at a Stress Ratio of 0.1

Figure 5.3 depicts the room temperature fatigue R-curves with a stress ratio of 0.1. One of the data sets shows the beginning of a plateau in SEERR, and thus fully developed fibre bridging, at around 95mm of delamination growth while the other does not show a plateau. This observation is also confirmed when looking at Figures 5.4 and 5.5. Here, it can be seen that for test F0.1\_UD\_RT\_01, the last two resistance curves overlap, indicating fully developed fibre bridging and the plateau seen in figure 5.3. For test F0.1\_UD\_RT\_02, it is observed that there is still spacing between the last two resistance curves and thus there is no plateau of fully developed fibre bridging reached.

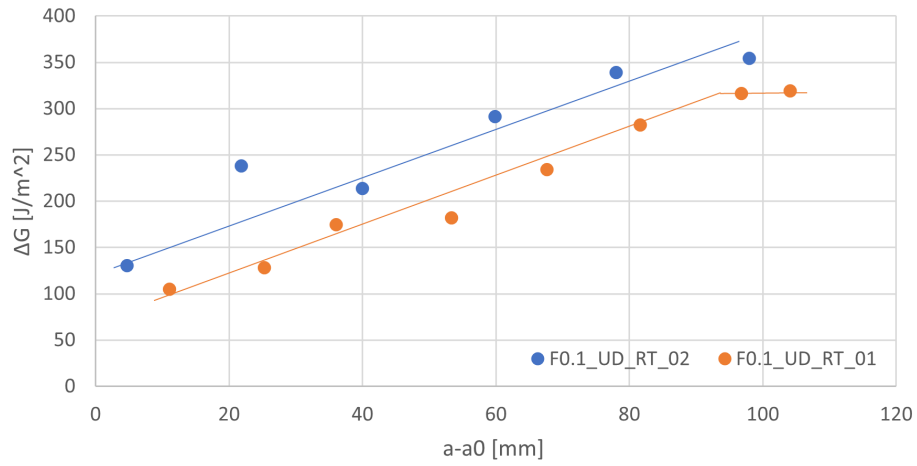


**Figure 5.3:** R-curves for tests F0.1\_UD\_RT\_01 and F0.1\_UD\_RT\_02 with  $R = 0.1$  and  $T =$  room temperature at  $da/dN = 1E-7$

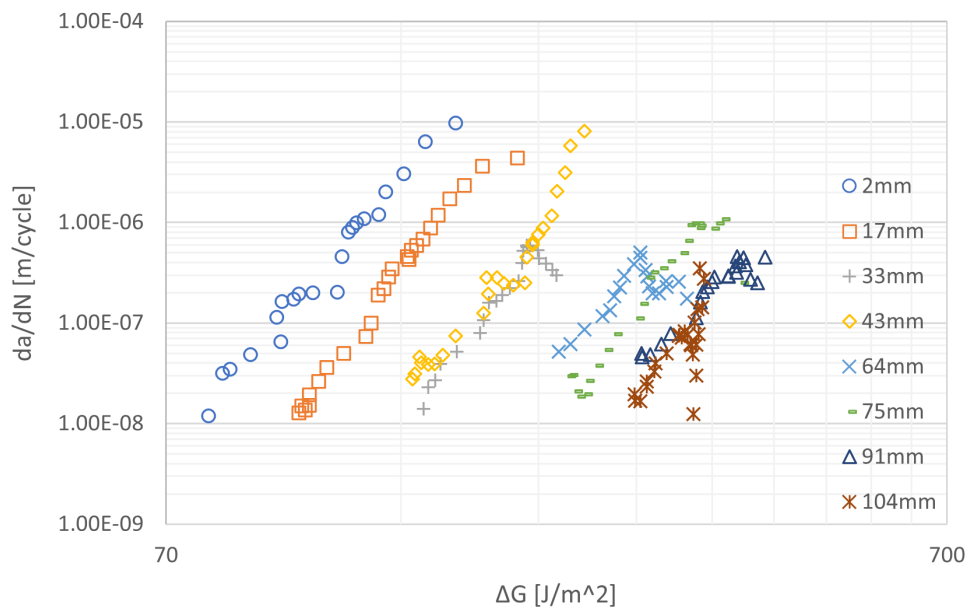


**Figure 5.4:** resistance curves for test F0.1\_UD\_RT\_01 with  $R = 0.1$  and  $T =$  room temperature at different precrack lengths

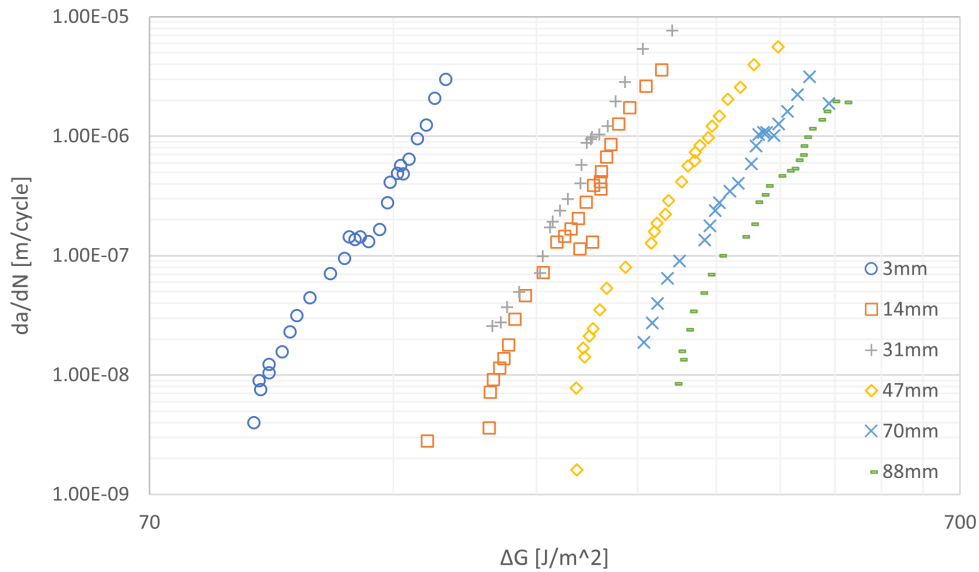


**Figure 5.5:** resistance curves for test F0.1\_UD\_RT\_02 with  $R = 0.1$  and  $T = \text{room temperature}$  at different precrack lengths; note: the resistance curve with precrack length of 14mm is out of place compared to the other resistance curves. This is due to a machine malfunction halfway through the test.

### 5.1.3 Fatigue Data at Stress Ratio of 0.5

In Figure 5.6, the fatigue R-curves for room temperature tests with stress ratio of 0.5 are given. For both tests, no final plateau region of fully developed steady state of fibre bridging is reached. For test F0.5\_UD\_RT\_02 however, a temporary plateau is reached between about 60mm and 80mm. This temporary plateau can also be seen in figure 5.7 where the resistance curves with precrack lengths of 46mm, 57mm and 70mm overlap.

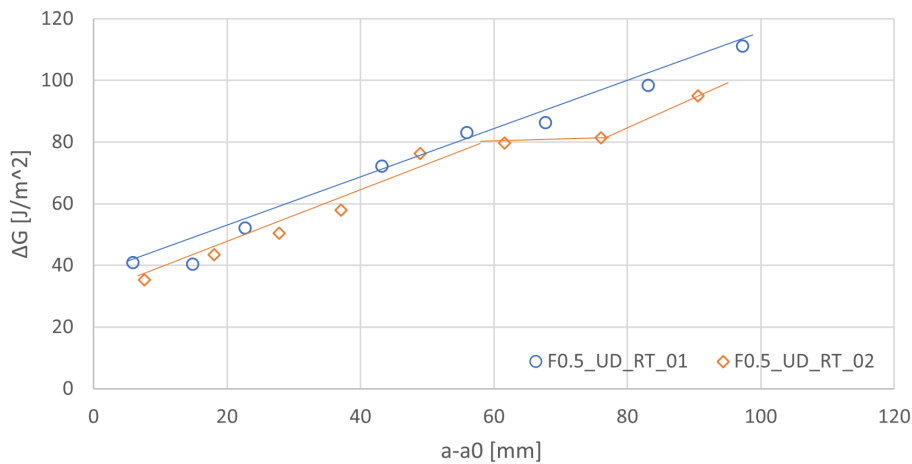


**Figure 5.6:** R-curves for tests F0.5\_UD\_RT\_01 and F0.5\_UD\_RT\_02 with  $R = 0.5$  and  $T = \text{room temperature}$  at  $da/dN = 1E-7$

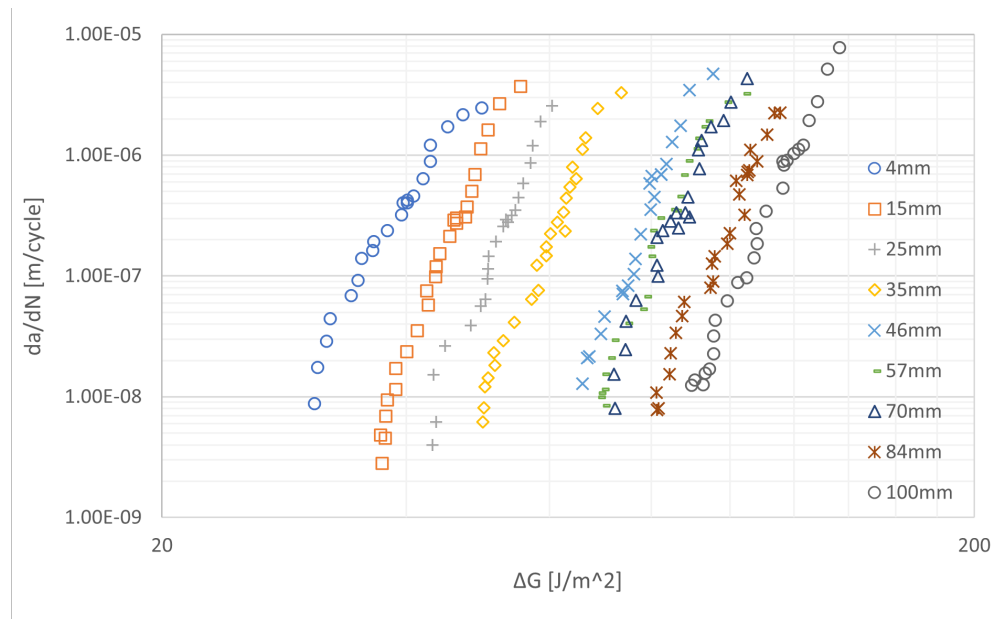


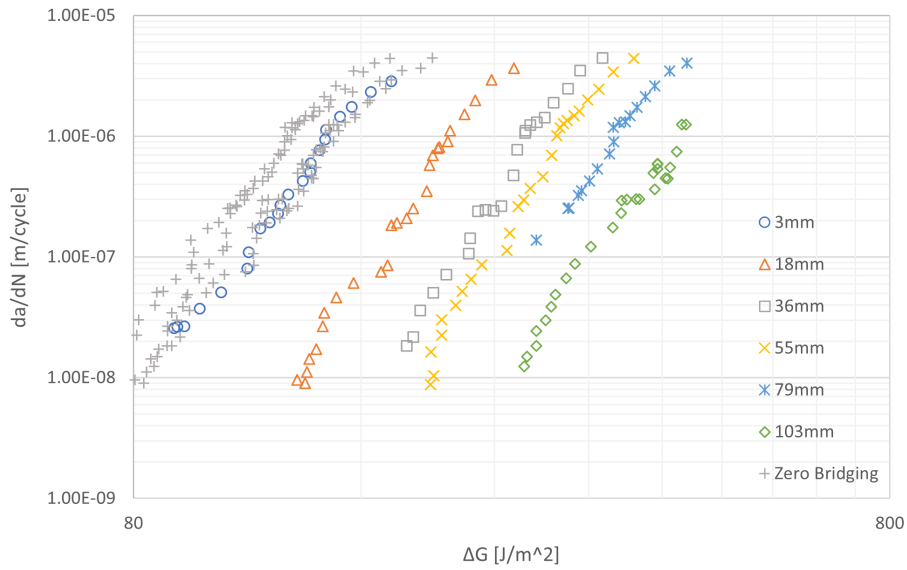
**Figure 5.7:** resistance curves for test F0.5\_UD\_RT\_02 with  $R = 0.5$  and  $T = \text{room temperature}$  at different precrack lengths

### 5.1.4 Concluding remarks

When reviewing the results for both quasi-static and fatigue tests at room temperature, it is observed that during quasi-static testing, a steady state of fibre bridging is reached after about 80mm of delamination growth. During fatigue testing, for both  $R=0.1$  and  $R=0.5$ , this plateau of steady state fibre bridging is not so obvious. At  $R=0.1$ , one of the tests shows the beginning of a plateau after about 95mm of delamination growth. For stress ratio 0.5, a temporary plateau is reached, but this disappears again when the test is continued. Later in Chapter 6, these room temperature results are compared to results gather by Yao for his PhD research [2].

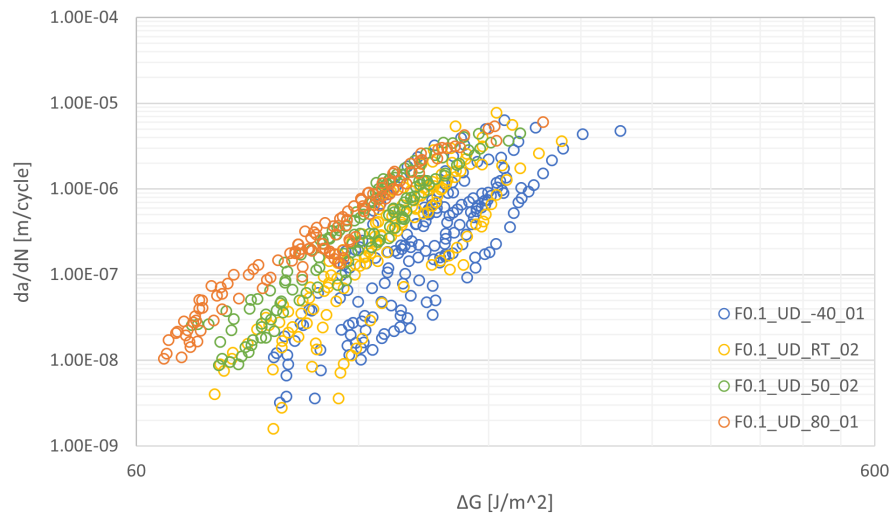
## 5.2 Temperature Influence on Delamination Resistance

To evaluate the influence of temperature on delamination resistance, a method proposed by Alderliesten [53] is used to generate delamination resistance curves. These 'zero bridging' resistance curves eliminate the influence of fibre bridging. In Figure 5.8, the comparison is made between such a zero bridging curve and the resistance curves with fibre bridging. With the increase of fibre bridging, the resistance curves move more to the right on the resistance graph. The zero bridging curve represents all resistance curves at different precrack lengths. Here, it can be seen that it does not have large shifts to the right on the resistance graph, but all data is much closer together.



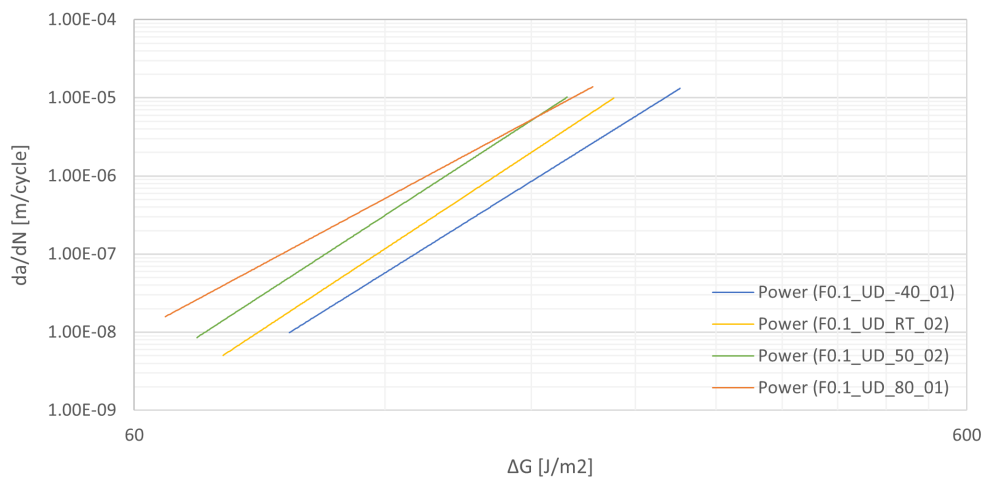
**Figure 5.8:** Comparison between resistance curves and the corresponding zero bridging curve for test F0.1\_UD\_50\_02 with  $R = 0.1$  and  $T = 50^\circ\text{C}$

Figure 5.9 shows the zero bridging curves for tests conducted at different temperatures. Because there are a lot of data points on a small space, it is hard to read the graph. However, a trend from right to left can be seen with increasing temperature. At  $80^\circ\text{C}$ , the difference with the other temperatures becomes larger with decreasing delamination growth rate.



**Figure 5.9:**  $\Delta G$  vs  $da/dN$  zero bridging curves at different temperatures

To make Figure 5.9 easier to read, in Figure 5.10 only the trendlines of the different zero bridging curves are shown. Here, the pattern that was observed earlier becomes clearer. At the beginning of the tests, at high  $da/dN$  values, it can be seen that at an ambient temperature of  $-40^{\circ}\text{C}$  the delamination growth rate at a certain SERR is lower compared to room temperature. The difference becomes smaller as the tests progress towards lower delamination growth rates. For elevated temperatures, the opposite is true. At high delamination growth rates, an ambient temperature of  $50^{\circ}\text{C}$  or  $80^{\circ}\text{C}$  causes a higher delamination growth rate at a certain SERR compared to room temperature, but no difference between  $50^{\circ}\text{C}$  and  $80^{\circ}\text{C}$  is observed. At lower delamination growth rates, the difference between room temperature and  $50^{\circ}\text{C}$  remains constant, but the difference in delamination growth rate at a certain SERR between  $80^{\circ}\text{C}$  and room temperature increases.



**Figure 5.10:**  $\Delta G$  vs  $da/dN$  zero bridging curves at different temperatures

Using energy principles, a more physical approach to delamination growth rate is taken. Zero bridging curves based on energy principles are determined as the left boundary of the interval in which the data is situated on a  $da/dN$  vs  $dU/dN$  graph. An example is given in Figure 5.11.

In Figure 5.12, the energy based zero bridging curves at different temperatures are depicted. Although the differences are small, a similar pattern to the fracture mechanics approach is found. At a given delamination growth rate, more energy is dissipated to continue delamination growth with decreasing temperature. This means delamination resistance increases with decreasing temperature and this delamination growth rate decreases with decreasing temperature. There is no difference between an ambient temperature of  $50^{\circ}\text{C}$  and  $80^{\circ}\text{C}$ . Similar to what was found using fracture mechanics the difference between high temperatures and low temperatures increases with decreasing delamination growth rate. The difference between  $-40^{\circ}\text{C}$  and room temperature decreases with decreasing delamination growth rate until at delamination growth rates of  $1\text{E-}7$  and below, the rate of energy dissipation at room temperature and at  $-40^{\circ}\text{C}$  is similar.

Based on both fracture mechanics and energy principles, it can be concluded that, excluding the influence of fibre bridging, delamination growth rate decreases with decreasing temperature.

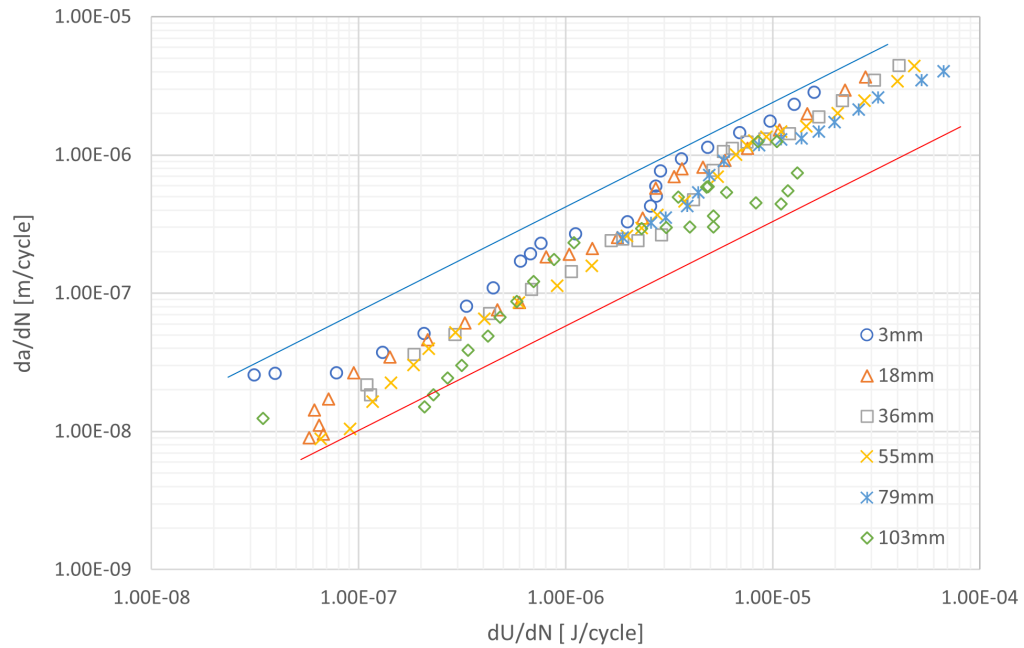


**Figure 5.11:**  $da/dN$  vs  $dU/dN$  graph with left zero bridging boundary and right maximum bridging boundary

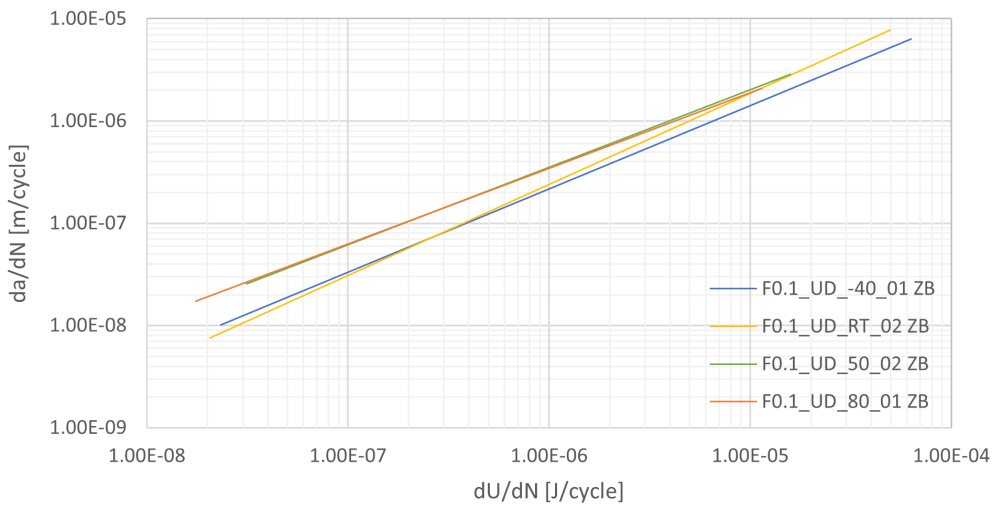


**Figure 5.12:**  $dU/dN$  vs  $da/dN$  zero bridging curves at different temperatures

## 5.3 Temperature Influence on Fibre Bridging

Before making a comparison of fibre bridging at the different temperatures that were tested, first the results at each temperature are given separately. When the effect of fibre bridging at each of the temperatures is established, a comparison can be made.

### 5.3.1 Fibre Bridging at $-40^{\circ}\text{C}$

The fatigue resistance curves with different fatigue precrack lengths from test F0.1\_UD\_-40\_01 performed at  $-40^{\circ}\text{C}$  are shown in Figure 5.13. The different resistance curves represent tests with different amounts of fibre bridging. With increasing precrack length, more fibre bridging occurs and the resistance curve shifts to the right on the resistance graph. This means that meaning at a certain SERR, the delamination growth rate decreases with increasing amounts of fibre bridging.

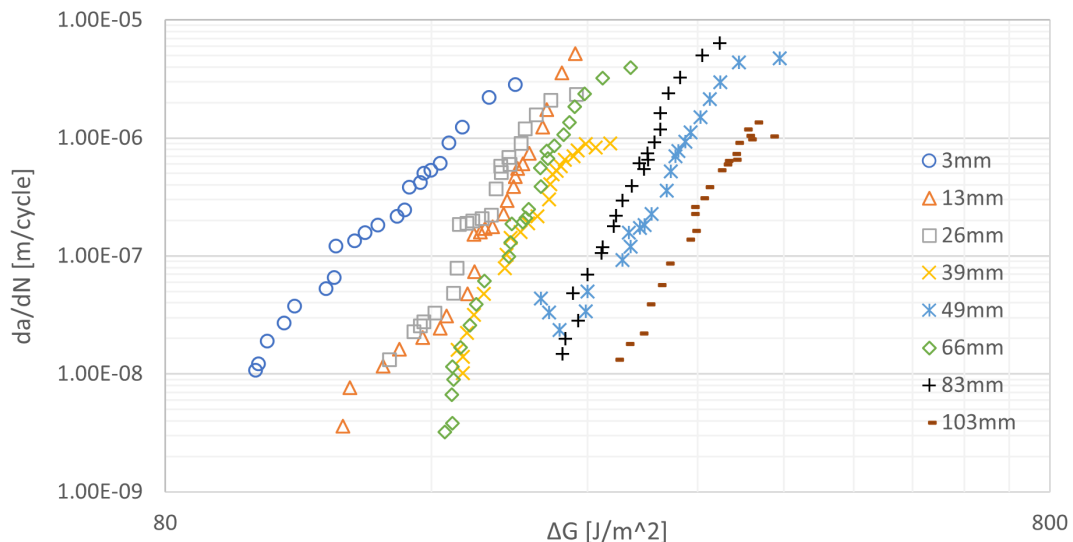


**Figure 5.13:** Resistance curves of test F0.1\_UD\_-40\_01 carried out at  $-40^{\circ}\text{C}$  with a stress ratio of 0.1 with different fatigue precrack lengths

In Figure 5.14, using the method proposed by Alderliesten [53] also used in the previous section, resistance curves have been translated on the resistance graph to a state in which there is no fibre bridging. From this analysis, data for certain precrack lengths is lifted out to be compared to the corresponding resistance curve where fibre bridging is included. Here, it is clearly visible that fibre bridging causes a larger shift to the right on the resistance graph and thus cause lower delamination growth rate at a certain SERR. It can also be seen that the larger the precrack length, and thus the more fibre bridging, the larger the shift of the resistance curve.

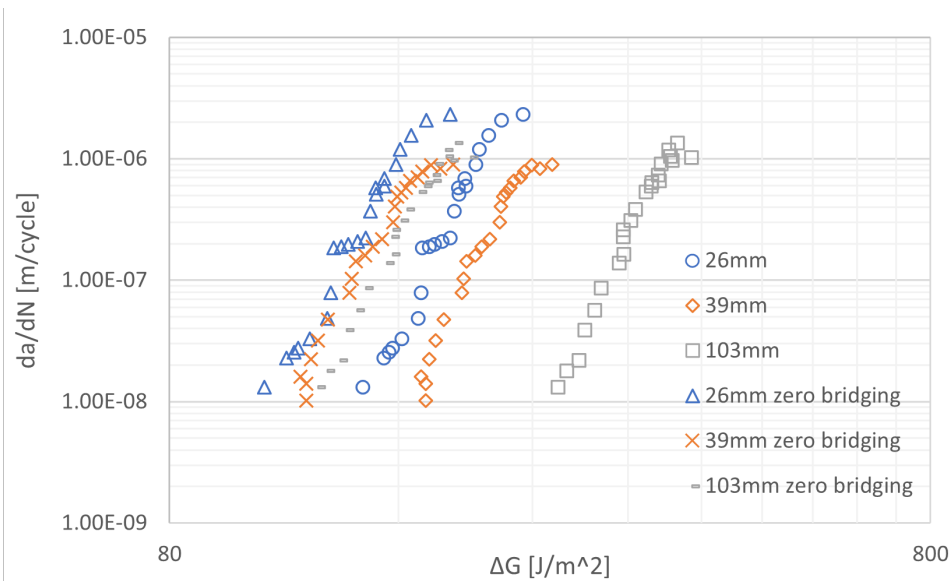


**Figure 5.14:** Comparison between zero bridging curve and resistance curve at certain fatigue precrack lengths

From Figures 5.13 and 5.14, it can be concluded that fibre bridging increases with increasing precrack length. Looking at Figure 5.13, no plateau, indicated by resistance curves coinciding, seems to be reached. To have a clearer view on this, in Figure 5.15 the fatigue R-curve at a  $da/dN$  value of  $1E-7$  and the quasi static resistance curve are shown.

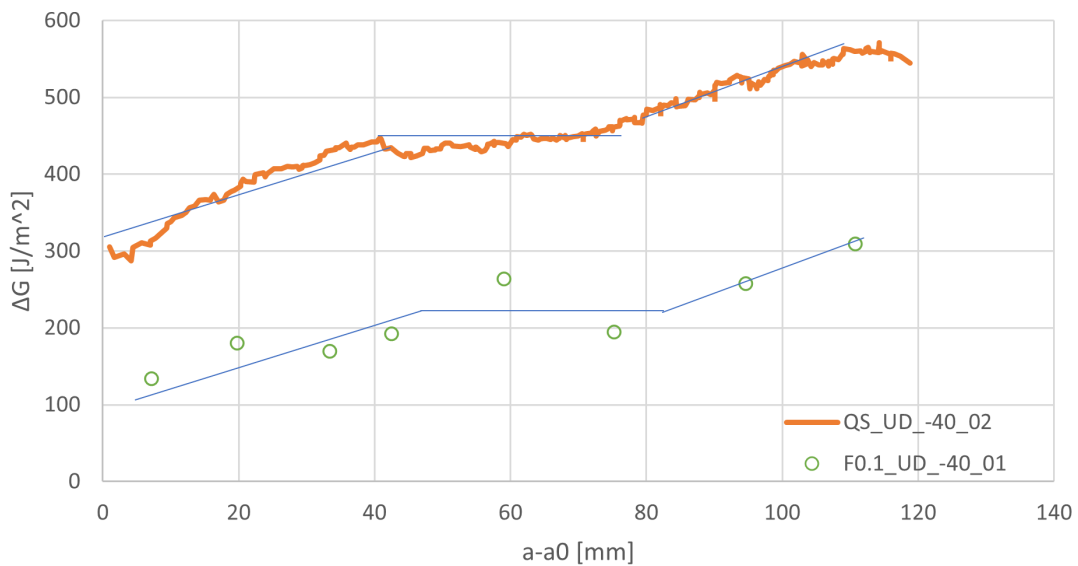


**Figure 5.15:** Quasi-static resistance curve and fatigue R-curve at a  $da/dN$  value of  $1E-7$

The fatigue R-curve in Figure 5.15 confirms what was already visible in the resistance curves. Fibre bridging does not reach a steady state at high  $a-a_0$  values. However, there is a steady state of fibre bridging between 40mm and 80mm of delamination length. When looking back to the resistance curves in Figure 5.13, it is noticed that the resistance curves with a precrack length of 39mm and 66mm coincide. Even the resistance curves with precrack lengths of 13mm and 26mm lie very close together. To confirm these findings, also the quasi-static resistance curve is drawn in Figure 5.15. Also during the quasi-static tests, there was a steady state of fibre bridging between 40mm and 60mm of delamination length after which it disappeared again. The quasi-static tests were ran until longer delamination lengths compared to the fatigue tests. Towards the end at 110mm of quasi-static delamination length, the resistance curve bends down again and suggests that a new steady state is reached. However, to make a definitive statement about this, experiments should be continued to longer delamination lengths and thus longer specimens are required.

To find a physical explanation for fibre bridging, besides fracture mechanics also a physics based approach using energy principles was used. In Figure 5.16, the resistance curves of test F0.1\_UD\_-40\_01 generated using energy principles are depicted. Here, the reality of delamination growth is illustrated in a very literal manner. When at a certain crack growth rate the resistance of the material is higher, there is a higher energy needed to continue the delamination. The different resistance curves at different fatigue precrack lengths shift on this graph from left to right with increasing precrack lengths. The left boundary indicated by the blue line is the point where there is no bridging, comparable to the zero bridging curves as shown in Figure 5.14. The right boundary signifies the point where most fibre bridging occurs. Seeing as the resistance curves differ more from the left boundary with increasing precrack length, it can be said that there is an increasing amount of fibre bridging and increase in delamination resistance proportional to the distance between the resistance curve and the left boundary.

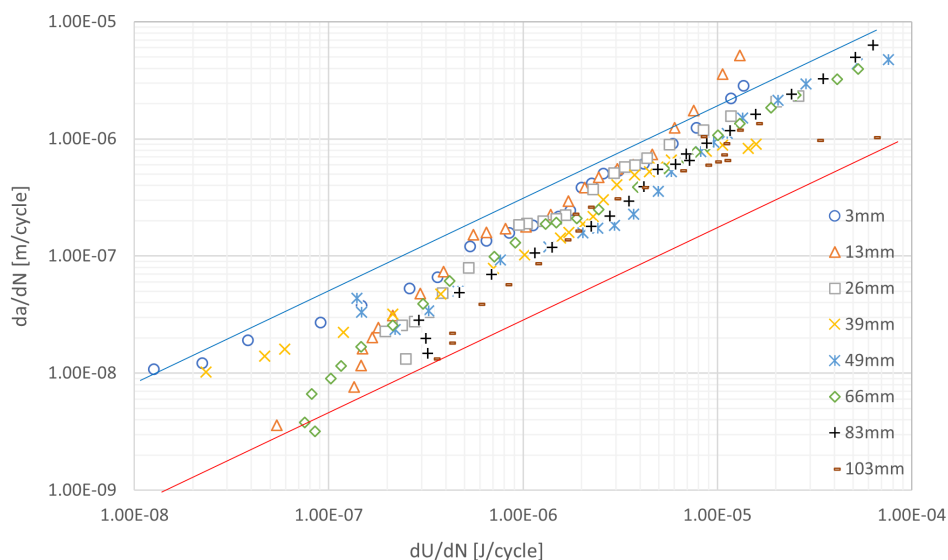


**Figure 5.16:** Resistance curves of test F0.1\_UD\_-40\_01 carried out at  $-40^{\circ}\text{C}$  with a stress ratio of 0.1 with different fatigue precrack lengths

To summarize, based on both fracture mechanics and energy principles it can be said that at  $-40^{\circ}\text{C}$ , fibre bridging has a large influence on fatigue delamination growth. It is shown that fibre bridging increases with increasing delamination length until a delamination length of 40mm after which fibre bridging reaches a steady state. When a delamination length of 60mm is reached, this steady state disappears again and the amount of fibre bridging increases. The quasi-static resistance curve suggests a new, higher level, steady state occurs at a delamination length of 110mm. Additional research is needed however to make definitive statements about this.

### 5.3.2 Fibre Bridging at $50^{\circ}\text{C}$

The data gathered with performing tests at  $50^{\circ}\text{C}$  can be analyzed in a similar manner as the data at  $-40^{\circ}$  was analyzed in the previous subsection. Here, the data is presented, observations are stated and conclusions are drawn.

In Figure 5.17, it can be observed that with increasing fatigue precrack length, resistance curves shift to the right on the resistance graph indicating a lower delamination growth rate at a certain SERR. When comparing the resistance curves to their 'zero bridging' counterparts in Figure 5.18, it is seen that this shift is caused by increasing amounts of fibre bridging. How fibre bridging develops can be deduced from Figure 5.19. Fibre bridging increases until a delamination length of 45mm. Here, fibre bridging reaches a steady state. At a delamination length of 90mm, this steady state disappears again and the amount of fibre bridging keeps increasing. The same conclusion can be made for quasi-static testing from the quasi-static resistance curve shown in Figure 5.19. This quasi-static resistance curve also suggests a second, higher level, stage of steady state of fibre bridging is reached at a delamination length of 115mm. However, to make a definitive statement about this experiments should be continued to longer delamination lengths and thus longer specimens are required.

The conclusions stated above are confirmed by looking at the energy principles in Figure 5.20. The resistance curves shift more to the right, away from the 'zero bridging' boundary, with increasing crack length and thus increasing amounts of fibre bridging occur with increasing crack length. Furthermore, it is also observed that the resistance curves with a precrack value of 36mm, 55mm and 79mm overlap for the most part, indicating a plateau in fibre bridging as also observed from Figure 5.19.

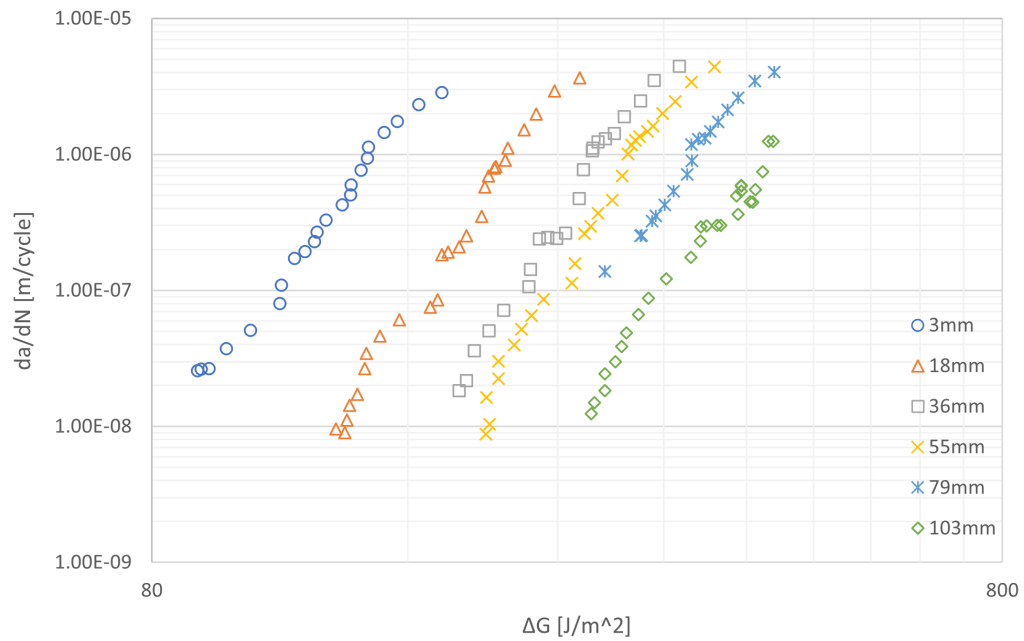


**Figure 5.17:** Resistance curves of test F0.1\_UD\_50\_02 carried out at 50°C with a stress ratio of 0.1 with different fatigue precrack lengths

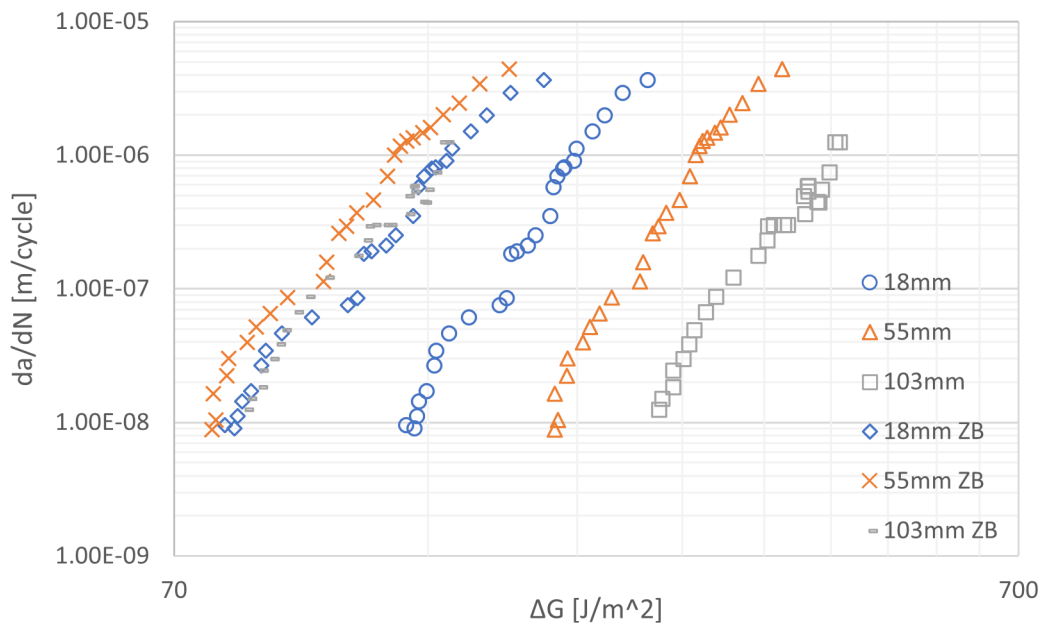


**Figure 5.18:** Comparison between zero bridging curves and resistance curves of test F0.1\_UD\_50\_02 at certain fatigue precrack lengths

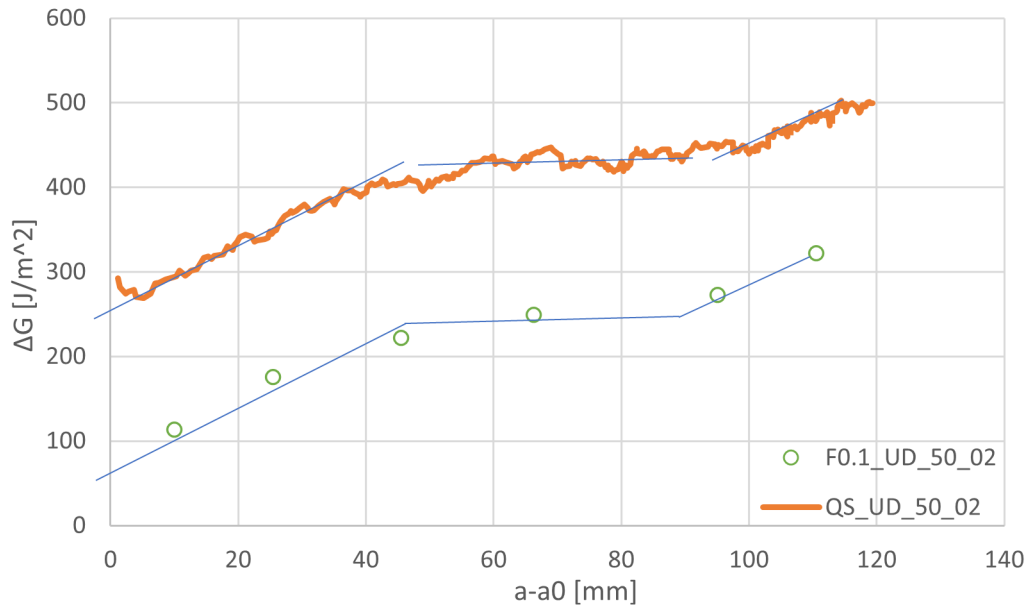


**Figure 5.19:** Quasi-static resistance curve and fatigue R-curve at a  $da/dN$  value of  $1E-7$

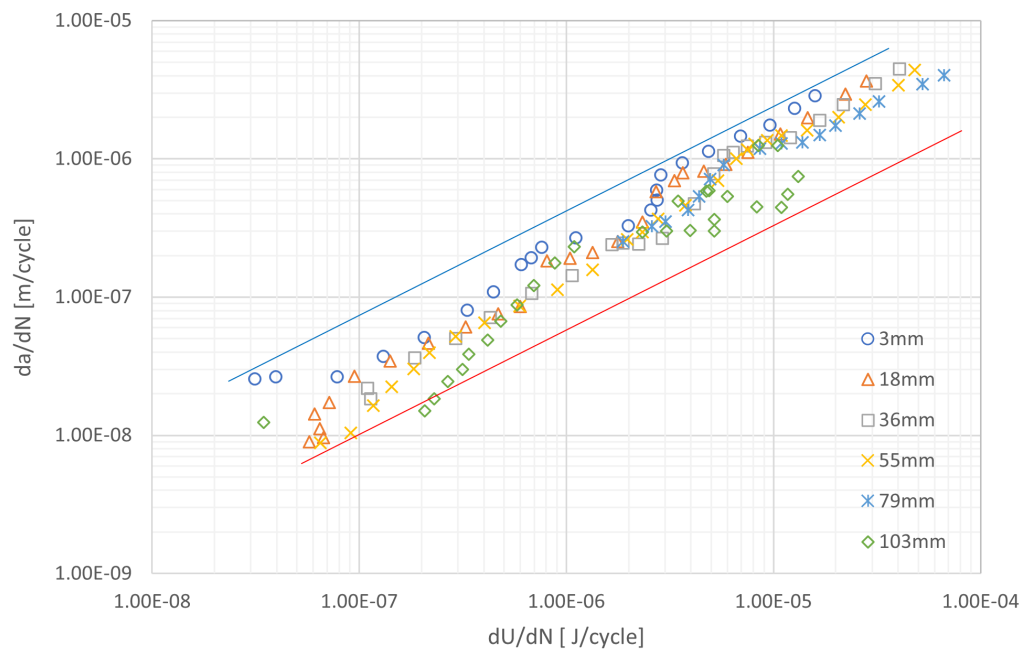


**Figure 5.20:** Resistance curves of test F0.1\_UD\_50\_02 carried out at  $50^{\circ}\text{C}$  with a stress ratio of 0.1 with different fatigue precrack lengths

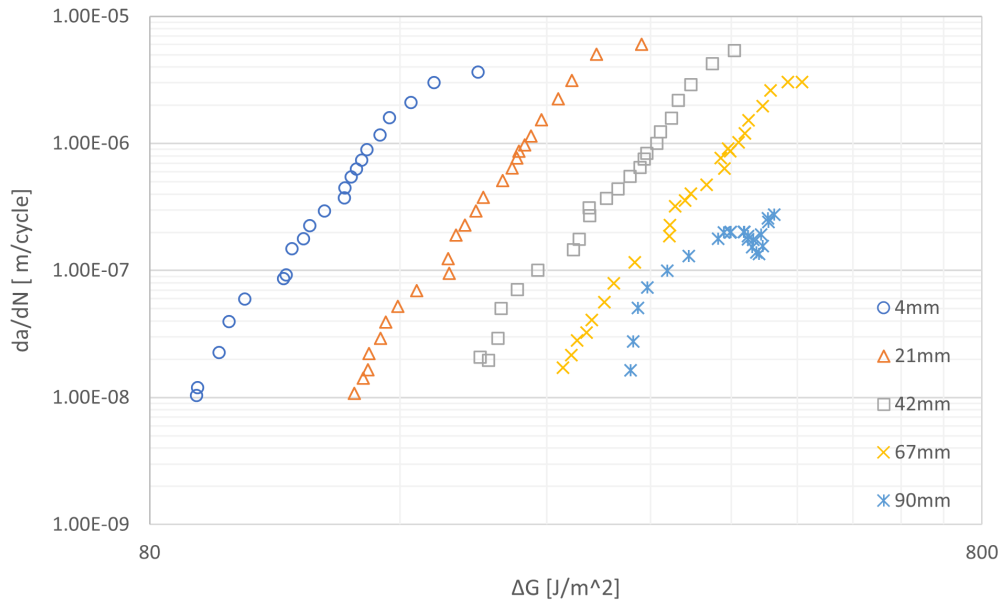


**Figure 5.21:** Resistance curves of test F0.1\_UD\_80\_01 carried out at  $-40^{\circ}\text{C}$  with a stress ratio of 0.1 with different fatigue precrack lengths

### 5.3.3 Fibre Bridging at $80^{\circ}\text{C}$

The data gathered with performing tests at  $80^{\circ}\text{C}$  can be analyzed in a similar manner as the data at  $-40^{\circ}$  was analyzed previously. Here, the data is presented, observations are stated and conclusions are drawn.

In Figure 5.21, it can be observed that with increasing fatigue precrack length, resistance curves shift to the right on the resistance graph. When comparing the resistance curves to their respective zero bridging curves in Figure 5.22, it can be concluded that this shift is caused by increasing amounts of fibre bridging.

How fibre bridging develops can be seen in Figure 5.23. To the contrary of the temperatures discussed earlier, at  $80^{\circ}\text{C}$ , fibre bridging does not seem to reach steady state. From the quasi-static resistance curve however, it can be deduced that during quasi-static testing a steady state of fibre bridging occurs between 60mm and 100mm of delamination growth. The resistance curve also suggests a second, higher level, steady state from 120mm of delamination growth onwards, but additional testing is necessary to make definitive statements about this.

To the contrary of tests at  $-40^{\circ}\text{C}$  and  $50^{\circ}\text{C}$ , at  $80^{\circ}\text{C}$ , the conclusions drawn from the fracture mechanics based analysis are not completely confirmed by the energy based approach shown in Figure 5.20. It is confirmed that the resistance curves shift more to the right, away from the 'zero bridging' boundary, with increasing crack length. Thus confirming increasing amounts of fibre bridging occur with increasing crack length. However, when looking at the resistance curves with precrack lengths of 67mm and 90mm, it can be seen that at a delamination growth rate of  $1\text{E}-7$ , both curves overlap. When translating this to Figure 5.19, this would mean a steady state of fibre bridging occurs from there.

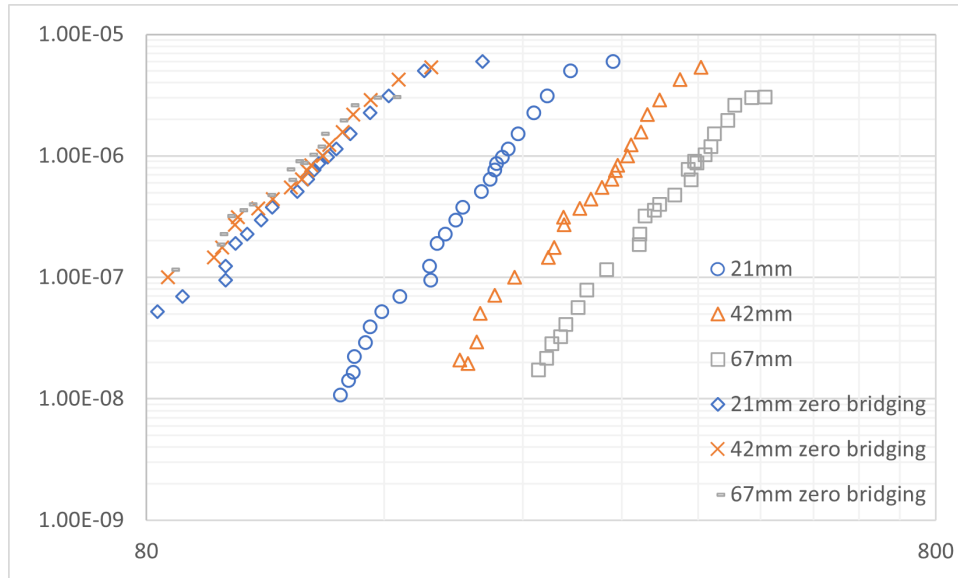


**Figure 5.22:** Comparison between zero bridging curves and resistance curves of test F0.1\_UD\_80\_01 at certain fatigue precrack lengths

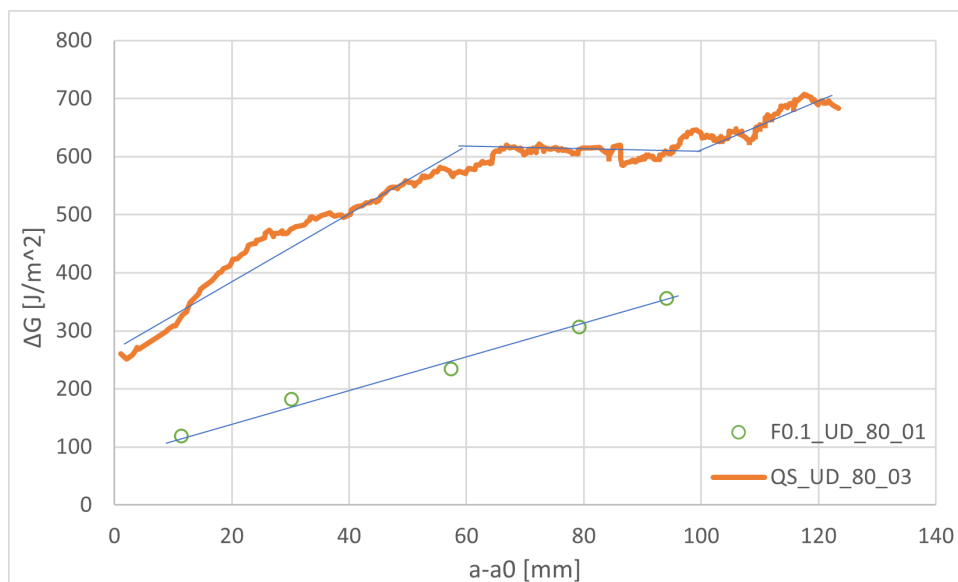


**Figure 5.23:** Quasi-static resistance curve and fatigue R-curve at a  $da/dN$  value of  $1E-7$

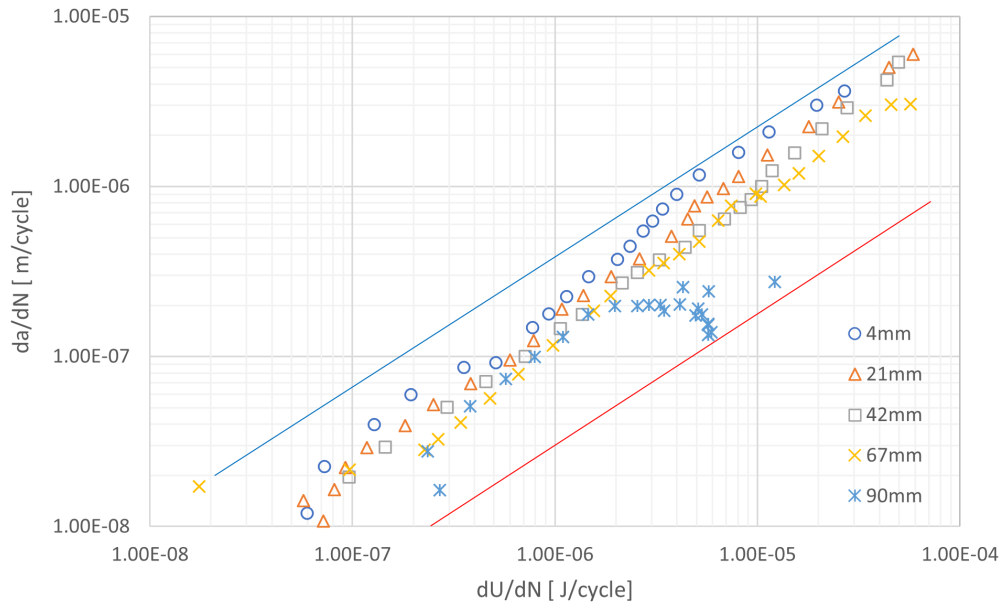


**Figure 5.24:** Resistance curves of test F0.1\_UD\_80\_01 carried out at 80°C with a stress ratio of 0.1 with different fatigue precrack lengths

### 5.3.4 Temperature comparison

After looking at what the influence of fibre bridging is on every temperature that was researched separately, now a comparison between the temperature is made to see if this influence changes with temperature.

In Figures 5.25 and 5.26, different resistance curves with similar precrack lengths and their zero bridging equivalent are compared. These single zero bridging curves have been lifted out of the zero bridging analysis. It can be seen that when excluding the influence of fibre bridging, delamination growth rate at a certain SERR decreases with decreasing temperature as was previously established in Section 5.2. When taking fibre bridging into account however, the opposite seems to be true. Now, delamination growth rate at a certain SERR increases with decreasing temperature. This is also illustrated in Figure 5.27. At small delamination lengths, where there is little to no fibre bridging, the SERR is smaller at elevated temperatures (50°C and 80°C). Between 35mm and 45mm of delamination growth, the SERR is approximately equal for all temperatures. At this point, the influence of fibre bridging has counteracted the influence of temperature on delamination growth rate excluding fibre bridging. After this point, the SERR is larger for elevated temperatures.

Based on the fracture mechanics analysis, it can thus be concluded that the influence of fibre bridging on fatigue delamination growth increases with increasing temperature.

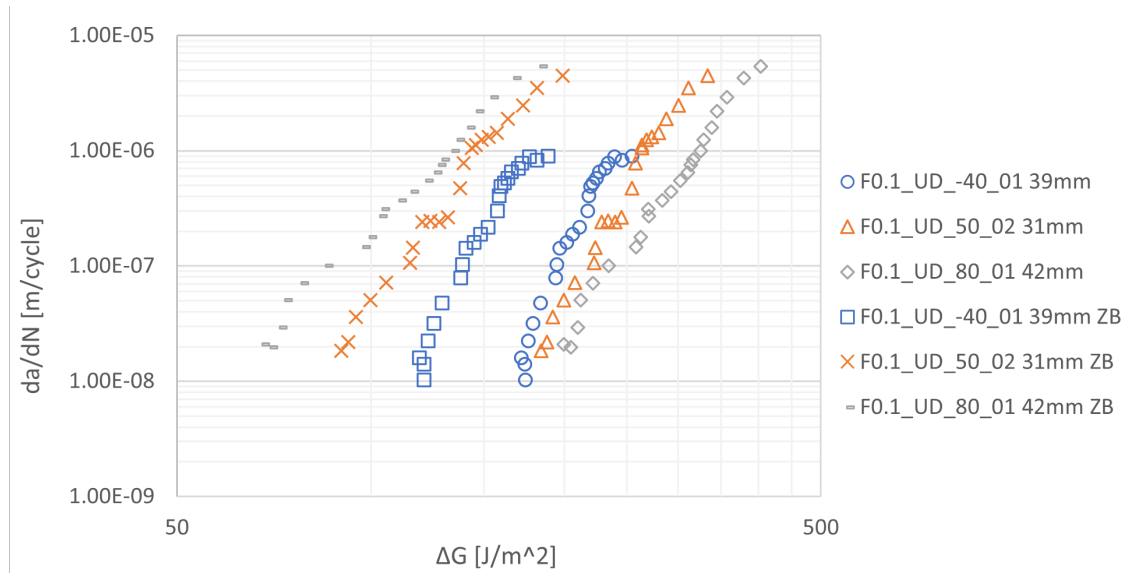


**Figure 5.25:** Temperature comparison of resistance curves with fatigue precrack lengths between 31mm and 42mm with their corresponding zero bridging curves

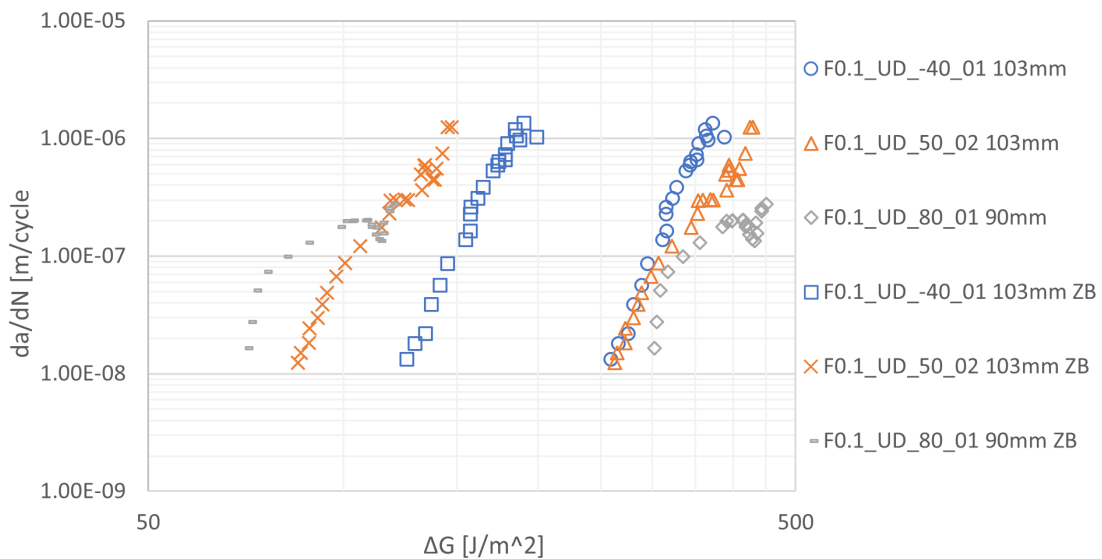


**Figure 5.26:** Temperature comparison of resistance curves with fatigue precrack lengths between 90mm and 103mm with their corresponding zero bridging curves

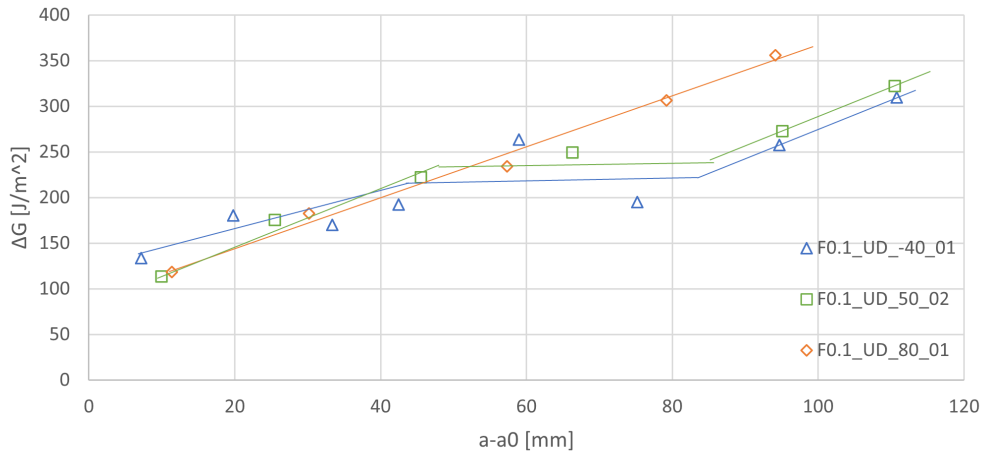


Figure 5.27: Temperature comparison of fatigue R-curves at a  $da/dN$  value of  $1E-7$

In Figure 5.28, energy principles are used to generate zero bridging and maximum bridging resistance curves. When looking at the zero bridging curves, indicated in the graph with 'ZB', delamination resistance is higher at lower temperatures, as was already established in Section 5.2. When looking at the resistance curves for maximum bridging, this effect has not been reversed. Different from the fracture mechanics analysis, the highest delamination resistance still occurs at the lowest temperature. At elevated temperature however, a change is noted. Whereas for the zero bridging case 50°C and 80°C resistance curves were identical, it is observed that delamination resistance at 80°C increased more with increasing amounts of fibre bridging compared to the 50°C case.

Fibre bridging thus increases delamination resistance more at both sub-zero and elevated extreme temperatures compared to less extreme temperatures.

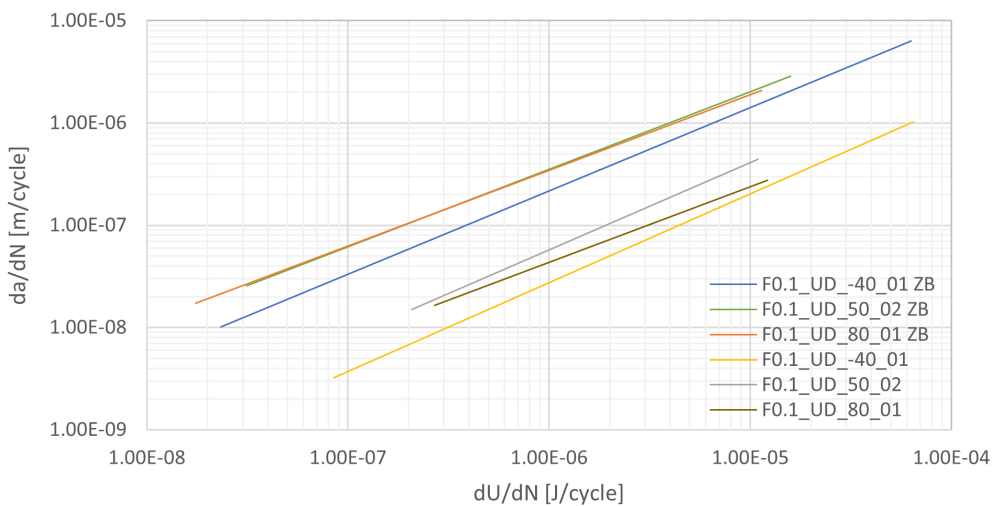
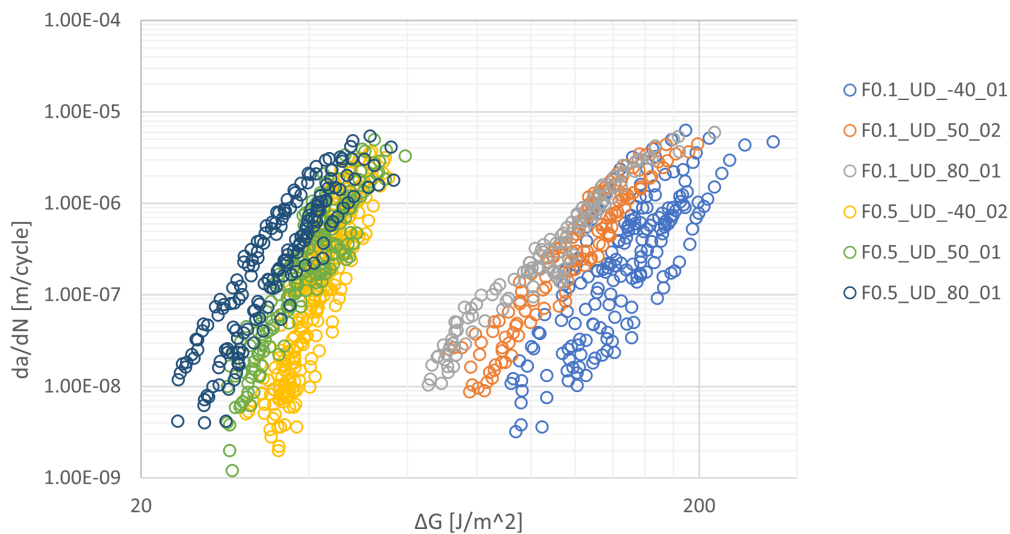


Figure 5.28: Temperature comparison of fatigue resistance curves at zero bridging and maximum bridging using energy principles

## 5.4 Temperature Influence on the Stress Ratio Effect

In Figure 5.29, zero bridging resistance curves at stress ratios 0.1 and 0.5 are compared at different temperatures. It immediately is obvious that there is a significant stress ratio effect. Furthermore, it is found that, for stress ratio 0.5 at high delamination growth rate values, there is not much difference in delamination resistance. However, at low delamination growth rate values delamination delamination growth rate at a certain SERR decreases with decreasing temperature. In Figure 5.30, only the trendlines of the zero bridging curves are shown. Here, the trends observed in Figure 5.29 are shown clearer. These findings are confirmed in Figure 5.31. Here, resistance curves at a precrack length between 90mm and 103mm are compared to their zero bridging counterparts at stress ratios 0.1 and 0.5. On the left three curves representing zero bridging curves at stress ratio 0.5, it is seen that at high  $da/dN$  values, there is not much difference between the temperatures. At lower  $da/dN$  values, a difference is seen in such a way that delamination growth rate at a certain SERR decreases with decreasing temperature like was also observed in Figure 5.30. Different from stress ratio 0.1 is that the influence of fibre bridging does not reverse the effect seen in the zero bridging curves. At  $R=0.5$ , it is found that it is found that delamination growth rate at a certain SERR decreases with extremer temperatures, both at elevated and sub-zero temperatures. An interesting observation is done that resistance curves including fibre bridging at  $R=0.5$  are in the same range as zero bridging curves at  $R=0.1$ . It is however not the case that  $R=0.5$  resistance curves match  $R=0.1$  zero bridging resistance curves at the same temperature.



**Figure 5.29:** Temperature comparison of zero bridging resistance curves at stress ratio 0.1 and stress ratio 0.5

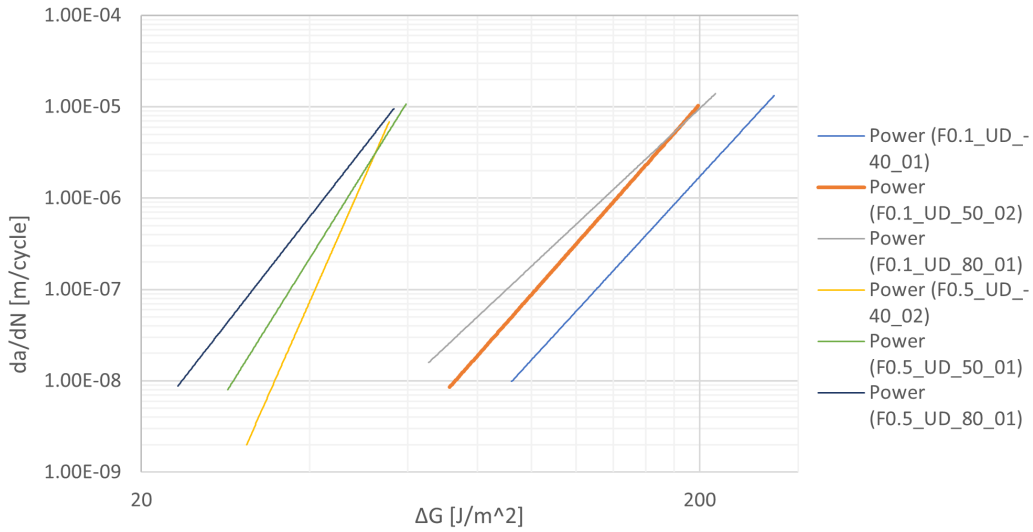


**Figure 5.30:** Temperature comparison of zero bridging resistance curves at stress ratio 0.1 and stress ratio 0.5

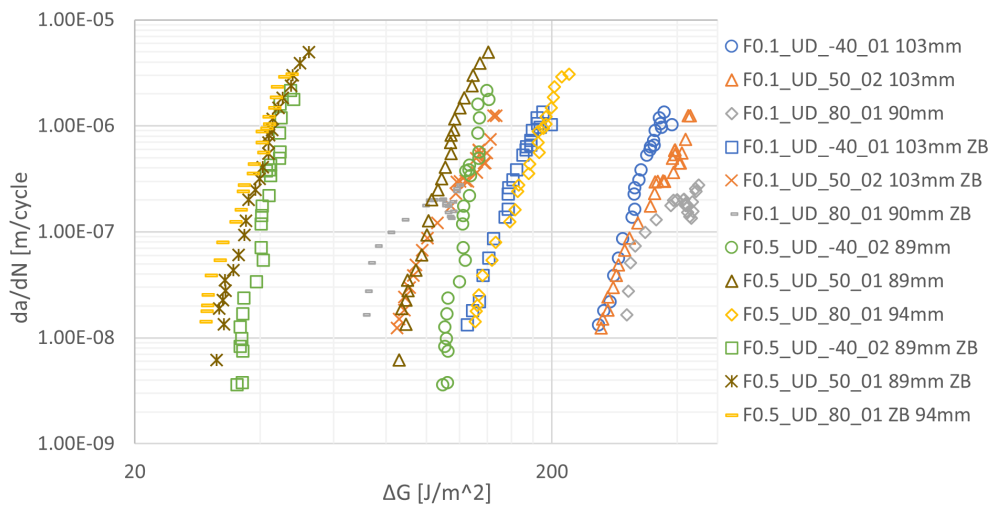


**Figure 5.31:** Temperature comparison of resistance curves with fatigue precrack lengths between 90mm and 103mm with their corresponding zero bridging curves at stress ratio 0.1 and stress ratio 0.5

When looking at the zero bridging resistance curves in Figure 5.32, it is seen that at high delamination growth rate values, the delamination resistance for different stress ratios is similar for all temperatures. At lower  $da/dN$  values however, it is found that at a certain  $da/dN$  value and a certain temperature the delamination resistance is higher at stress ratio 0.5 compared to stress ratio 0.1. The difference between the two stress ratios is bigger at  $-40^{\circ}\text{C}$  and  $80^{\circ}\text{C}$ . It can thus be said that at a certain temperature and  $da/dN$  value and temperature, delamination resistance increases with increasing stress ratio. This increase is bigger at more extreme temperatures

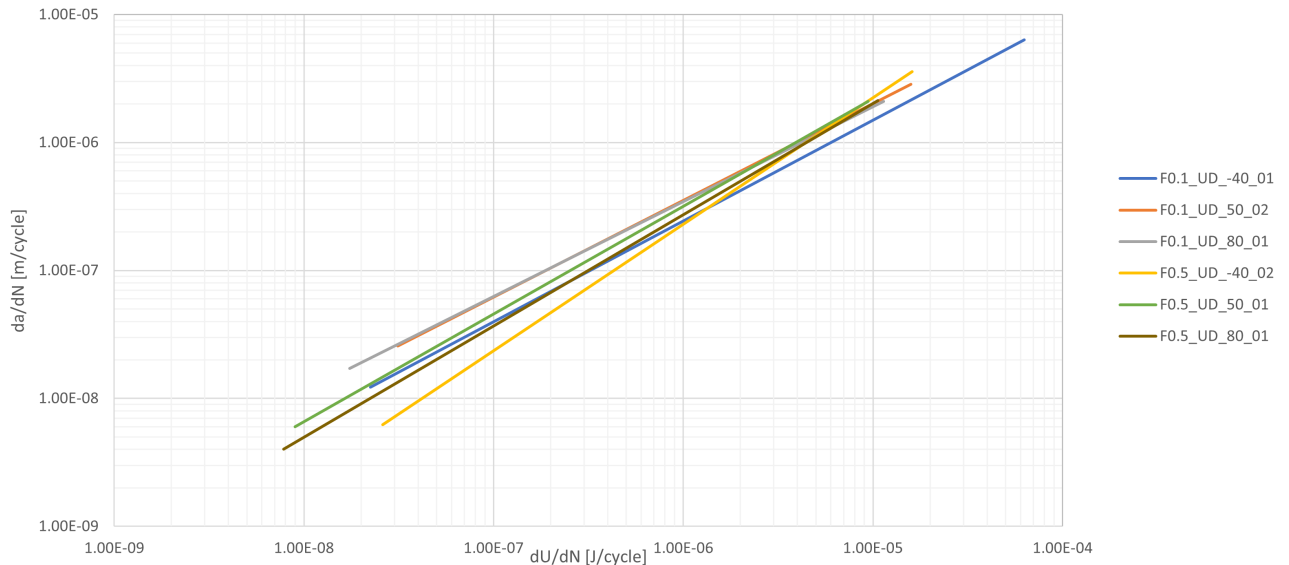


**Figure 5.32:** temperature comparison of fatigue resistance curves at zero bridging using energy principles at stress ratio 0.1 and stress ratio 0.5

In Figure 5.33, the rightmost boundaries of  $dU/dN$  vs  $da/dN$  resistance curves at different temperatures and different stress ratios is given. This boundary indicated maximum fibre bridging. Here, it is found that for low delamination growth rates, a similar stress ratio effect compared to Figure 5.32 is found. At higher delamination growth rates, the opposite from the zero bridging curves is true. The differences between the stress ratios are higher compared to lower delamination growth rates and this increase is bigger at more extreme temperatures.

From the physical approach to delamination growth it can be concluded that there is a stress ratio effect which is bigger at more extreme temperatures. Fibre bridging causes the stress ratio effect to be more outspoken at extreme temperatures compared to the zero bridging case. From the fracture mechanics approach, it can be said that excluding fibre bridging the difference in delamination resistance between different stress ratios increases with decreasing temperatures. When including fibre bridging however, it is found that that the effect of stress ratio on delamination resistance decreases towards the extremities of the temperature interval that was investigated.

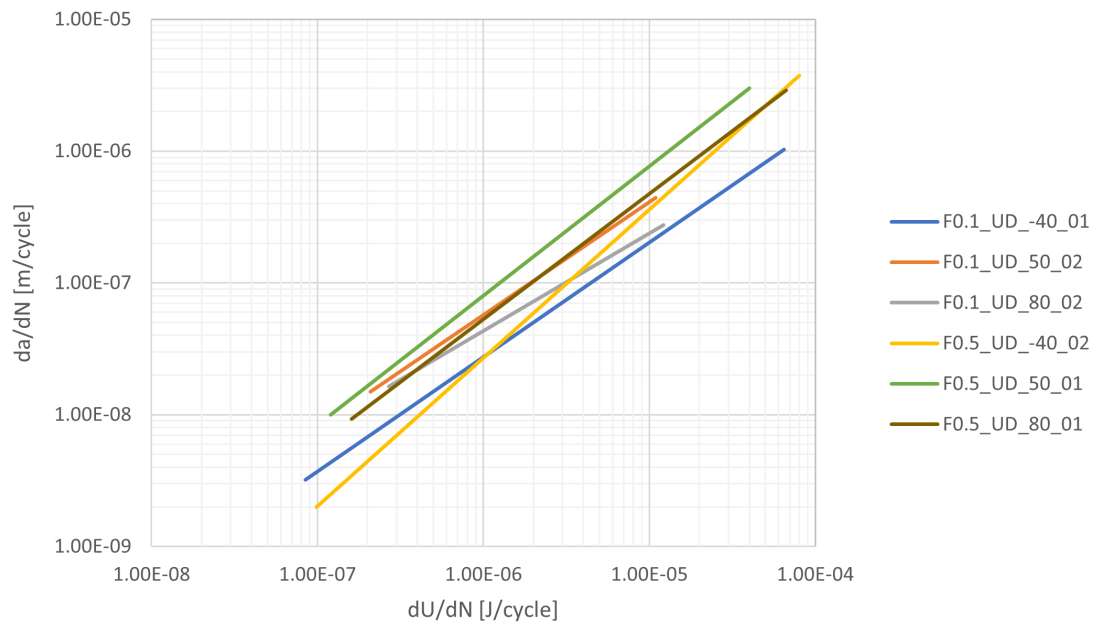


**Figure 5.33:** temperature comparison comparison of fatigue resistance curves at maximum using energy principles at stress ratio 0.1 and stress ratio 0.5



---

# Chapter 6

---

## Discussion

In this chapter, the results provided in Chapter 5 are discussed. In Section 6.1, the results of the comparison with data gathered by Yao [2] are discussed. Section 6.2 elaborates on temperature influence on delamination resistance. In section 6.3, the influence of temperature on fibre bridging is explained. Finally, Section 6.4 discusses the temperature influence on the stress ratio effect.

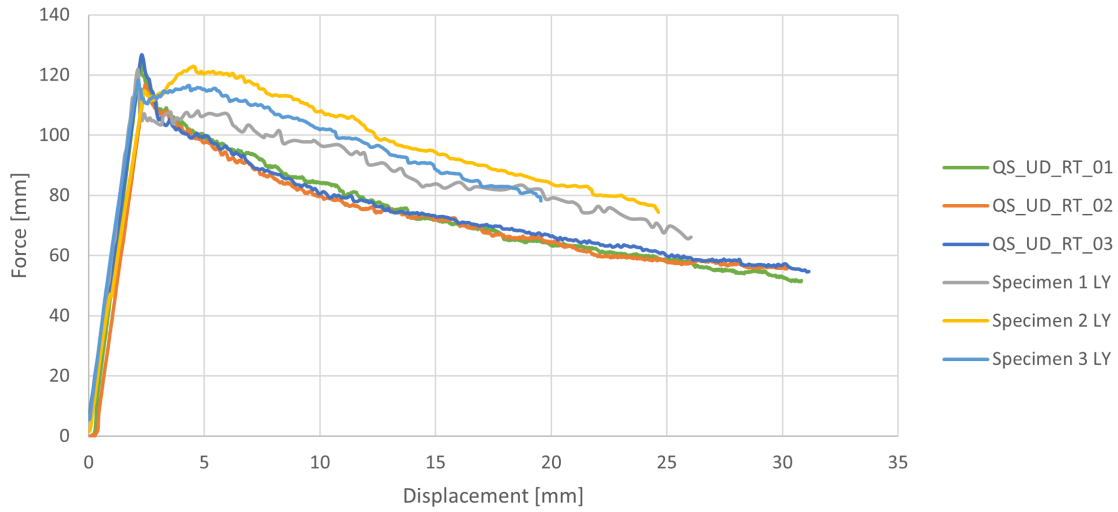
### 6.1 Room Temperature Data

In this section, the room temperature results are compared to results obtained by Yao [2]. The comparison with Yao [2] aims at seeing if his results can be reproduced. First, the quasi-static test data are compared. After that, the fatigue data at a stress ratio of 0.1 are compared and finally, the fatigue data at a stress ratio of 0.5 are compared.

#### 6.1.1 Quasi-static data

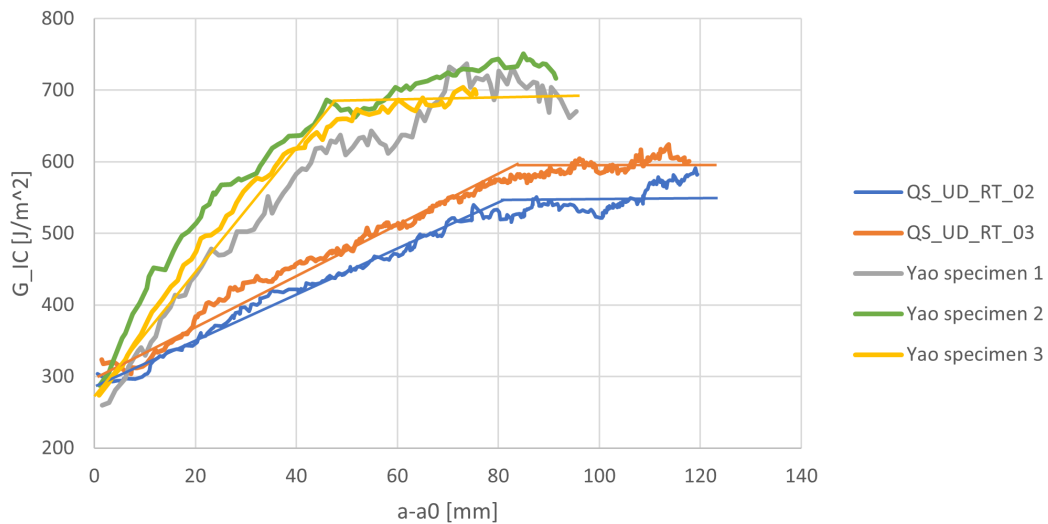
In Figure 6.2, force-displacement curves are compared. The force-displacement curves obtained in this research project are almost identical. When comparing to Yao's data however, a clear difference can be seen. At the point of delamination initiation, where the force starts to decrease, Yao's data shows a small decrease in force after which it increases again. This means the force is too small to continue delamination growth so the force increases before delamination continues.

When looking at the quasi-static resistance curves given in Figure 6.2, it is shown that the resistance curves of tests performed in this research project are similar to each other and the resistance curves generated by Yao are similar to each other. All tests, both from Yao's experiments and this research's experiments, have a similar initial  $G_{IC}$  value. However, the slope of the curves is different. The slope of the curves generated by Yao is steeper and the SERR reaches a plateau value sooner. This is indicated by the straight lines drawn on



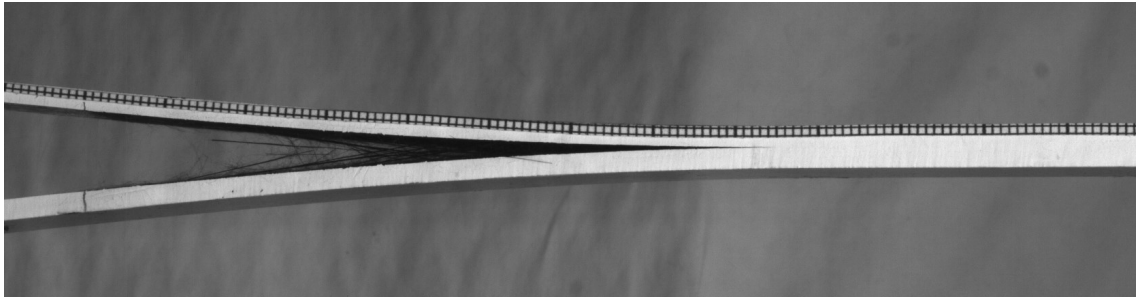
**Figure 6.1:** Force displacement curves of all QS tests performed at room temperature and of tests performed by Yao

Figure 6.2. As Yao indicates in his PhD research [2], this plateau was reached after 50mm of delamination growth. In this research however, this plateau is only reached after 80mm of delamination growth. The SERR value at which the plateau situates itself is between  $650 J/m^2$  and  $750 J/m^2$  for Yao's experiments and between  $550 J/m^2$  and  $600 J/m^2$  experiments carried out in this research project.



**Figure 6.2:** Quasi-static resistance curves of all QS tests performed at room temperature and of tests performed by Yao

This difference in results is caused by a difference in fibre bridging. At the start of a test, where the initial  $G_{IC}$  value is established, there is no fibre bridging. When the delamination grows, fibre bridging occurs in the wake of the delamination front which causes the  $G_{IC}$  value to increase with increasing delamination length. When fibre bridging reaches a steady state, the  $G_{IC}$  value reaches the aforementioned plateau value. At this point, the area in which fibre bridging occurs no longer increases. This difference in fibre bridging is shown in Figures 6.3 and 6.4. These show the side view of a specimen from a test from this research and a specimen tested by Yao respectively. The specimen tested by Yao shows more fibre bridging compared to the specimen tested during this research.



**Figure 6.3:** Side view of a specimen tested during the experimental phase of this research project showing signs of fibre bridging



**Figure 6.4:** Side view of a specimen tested by Yao showing signs of fibre bridging

The conclusion Yao drew, namely that fibre bridging occurs and reaches a steady state [2], can also be drawn here. The delamination length and SERR value at which this occurs are different however.

### 6.1.2 Fatigue data at a stress ratio of 0.1

In Figure 6.5, a comparison of test 'Specimen 7' performed by Yao and test F0.1\_UD\_RT\_02 performed in this research project is presented. These tests consisted of repeated fatigue tests on the same specimen at a stress ratio of 0.1 to investigate delamination growth with different amounts of fibre bridging. It shows that for similar fatigue precrack lengths, the resistance curves are comparable to each other.

Yao concluded that the resistance curves for the different fatigue precrack lengths shift from left to right on the resistance graph with increasing amount of fibre bridging since the crack growth rate  $da/dN$  decreases at a given  $\Delta G$  [2]. This happens until fibre bridging reaches steady state, similar to the quasi-static results discussed earlier. This plateau value is also shown in Figure 6.6.

Comparing this to the results from room temperature tests in this research, a clear difference is seen. Where 'specimen 7' from Yao's research shows a steady state of fibre bridging, this is not seen in test 'F0.1\_UD\_RT\_02'. In both Figures 6.5 and 6.6, no signs of a steady state of fibre bridging are seen.

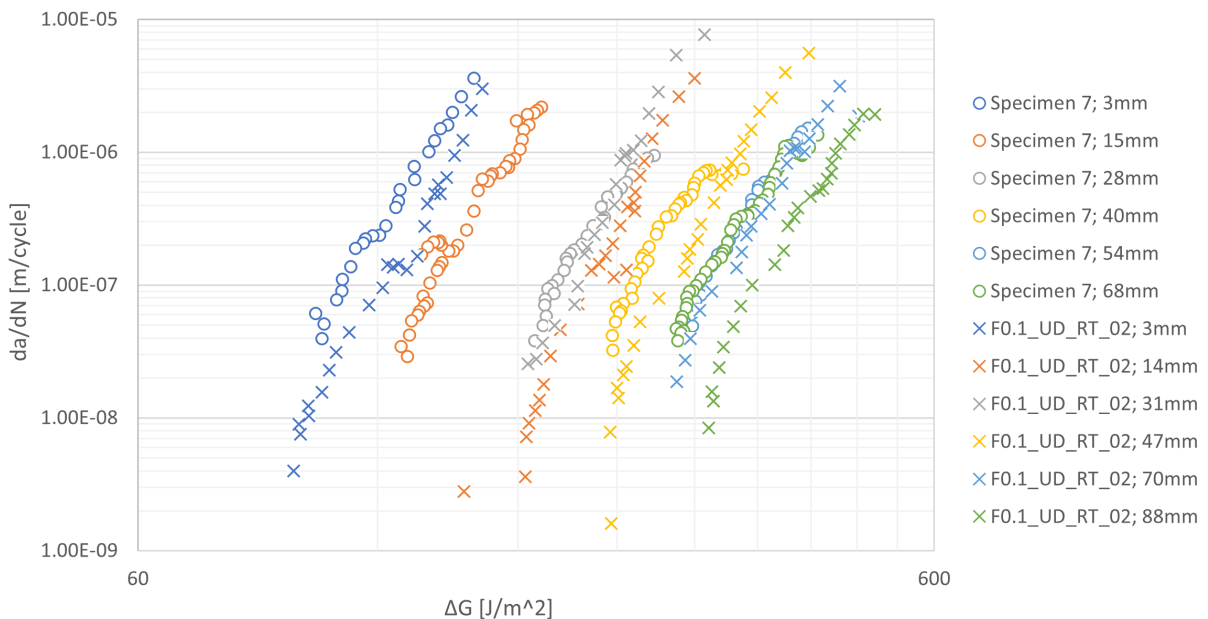


**Figure 6.5:** Resistance curve of fatigue tests specimen 7 and F0.1\_UD\_RT\_02 at stress ratio 0.5 with different fatigue precrack lengths

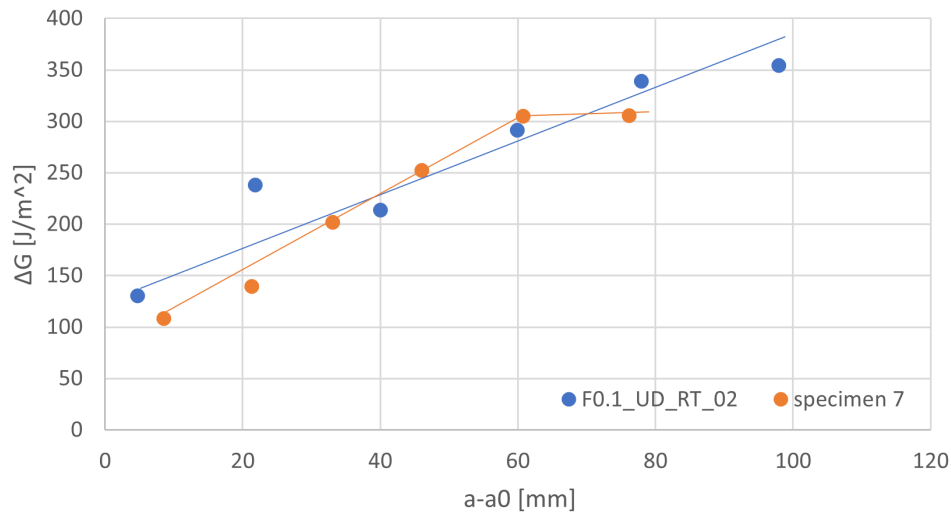


**Figure 6.6:** R-curve of fatigue tests specimen 7 and F0.1\_UD\_RT\_02 at stress ratio 0.5 and  $da/dN$  of  $1.0E-7$

### 6.1.3 Fatigue data at a stress ratio of 0.5

In Figure 6.7, a comparison between specimen 10, from the work of Yao [2], and F0.5\_UD\_RT\_02 is made. Whereas for the tests at a stress ratio of 0.1 there were clear similarities between the resistance curves at the same fatigue precrack lengths, here no such similarities are found. The difference in  $\Delta G$  values at certain  $da/dN$  values become larger with increasing precrack length. Both test results show similar behaviour at a qualitative level, but at a quantitative level they differ. For both tests, the resistance curves shift to the right of the resistance graph with increasing precrack length, and increasing amount of fibre bridging. Fibre bridging reaches a steady state where the resistance curves are closer together. However, when the precrack length increases further, this steady state disappears and the distance between resistance curves increases again. This is supported by Figure 6.8. At an  $a - a_0$  value of 30mm and 50mm for specimen 10 and F0.5\_UD\_RT\_02 respectively fibre bridging reaches a steady state. At 50mm and 75mm for specimen 10 and F0.5\_UD\_RT\_02 respectively, this steady state disappears again.

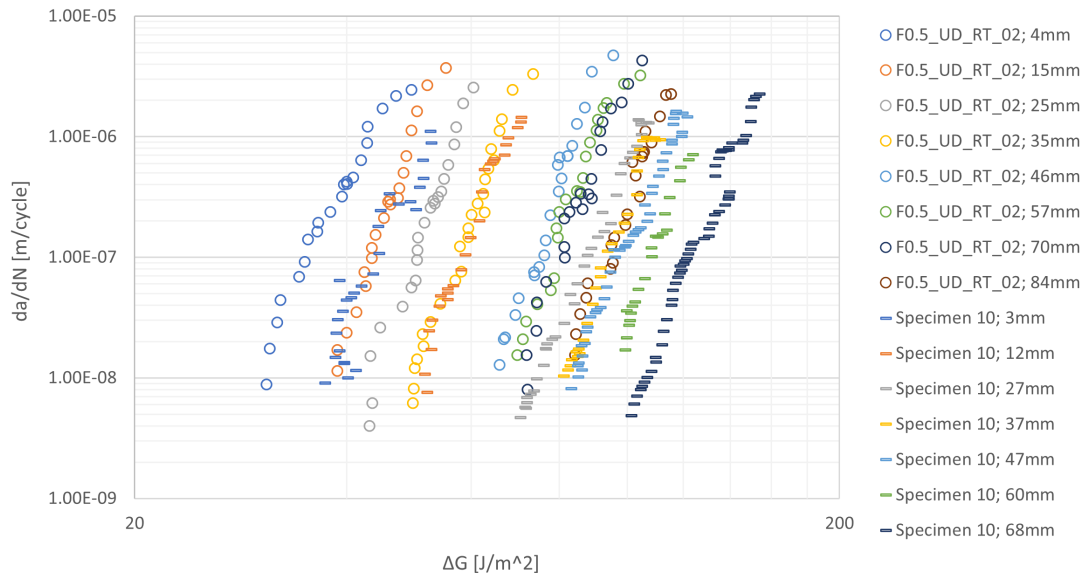


**Figure 6.7:** Resistance curve of fatigue tests specimen 10 and F0.2\_UD\_RT\_02 at stress ratio 0.1 with different fatigue precrack lengths

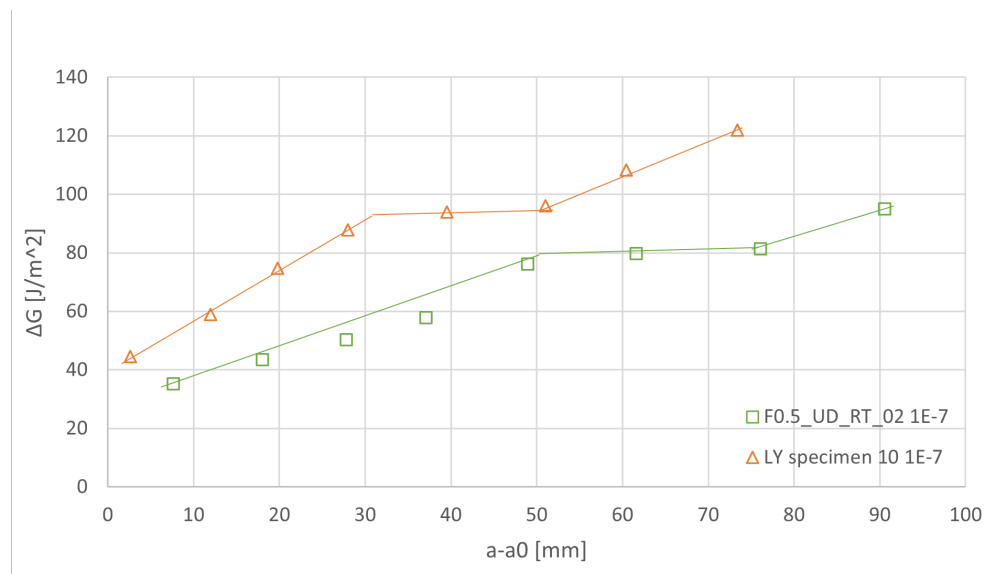


**Figure 6.8:** R-curve of fatigue tests specimen 10 and F0.2\_UD\_RT\_02 at stress ratio 0.1 and  $da/dN$  of  $1.0E-7$

#### 6.1.4 Concluding statements

It can be said that when the research by Yao and this research project are viewed individually, they reach the same conclusion on a qualitative level. From both results, it can be concluded that with increasing delamination length, the amount of fibre bridging increases until it reaches steady state. The increasing amount of fibre bridging increases the delamination resistance. When fibre bridging reaches steady state, the delamination resistance no longer increases.

The rate at which the amount of fibre bridging increases and the point where steady state is reached, if steady state is reached, is different for both data sets however. Although there is a difference, there is the consistency that fiber bridging increases slower in tests performed in this research compared to tests performed by Yao. This is due to the fact that after manufacturing, there was less fibre nesting in the composite laminate.

## 6.2 Temperature Influence on Delamination Resistance

Fatigue delamination growth rate at a certain SERR was found to decrease with decreasing temperature. This is supported by both analysis through fracture mechanics and by the physical approach using energy principles.

For evaluating the influence of temperature on delamination resistance, the influence of fibre bridging had to be excluded. In this research project, for SERR based resistance curves, this was done using a method proposed by Alderliesten [53]. For the energy based approach, this 'zero bridging' resistance curve was found by the left boundary of the interval in which all resistance data is situated as described by Yao [2].

Another approach was taken by Gregory and Spearing [62]. They developed a model to separate the SERR contributions of fibre bridging and propagation of a crack or delamination in resin. When applying this model to their data gathered in fatigue delamination testing at 149°C and 24°C, they came to the same conclusion as was made from this research. Namely that higher crack propagation rates, or lower resistance to delamination, was observed at higher temperatures.

Sjörge and Asp [63] took a physical approach for excluding fibre bridging. For their research, they used a layup with a 5° and 0° interface where the crack occurred. With this interface, they observed almost no fibre bridging while maintaining properties close to unidirectional properties. They performed tests at room temperature and at 100°C. Although they don't explicitly describe it in their report, their results showed a 50% lower SERR threshold for fatigue loading compared to room temperature.

When reviewing past and present studies, the same phenomenon was observed by different researchers. When excluding fibre bridging, fatigue delamination growth rate increases with increasing temperature.

## 6.3 Temperature Influence on Fibre Bridging

In general, it can be said that fibre bridging has a large influence on fatigue delamination growth across all temperatures. The amount of fibre bridging increases with increasing fatigue delamination length although it can reach a plateau at certain delamination lengths. This steady state does not always remain. When the delamination length keeps increasing, fibre bridging can start increasing again. The quasi-static resistance curves suggest a second, higher level, stage of steady state fibre bridging occurs at a certain point. However, from the experiments conducted in this research project it is not possible to make any definitive statements about this. To investigate this, one should continue a test to longer delamination lengths. Testing to delamination lengths above 120mm while making sure the specimens are not destroyed will require longer specimens.

The increase of fibre bridging with increasing delamination length is confirmed by resistance curves generated based on energy principles. Looking for the steady state of fibre bridging is very hard considering that on energy principles based resistance curves the data for different fatigue precrack lengths is very condensed.

When comparing the influence of fibre bridging on fatigue delamination growth over the different temperatures that were investigated, it was found that the effect temperature has on fatigue delamination growth is opposite of the effect it has on fibre bridging. When excluding fibre bridging, delamination growth rate at a certain SERR decreased with decreasing temperature. When fibre bridging is taken into account however, the opposite is true. The effect of fibre bridging on the delamination growth increases with increasing temperature, meaning that at higher temperatures fibre bridging has a larger effect on delamination growth.

When using energy principles as a basis for analyzing delamination growth, the outcome was somewhat different. Here, it was found that for both high and low extreme temperatures (80°C and -40°C), delamination growth showed a larger decrease with developing fibre bridging compared to temperatures closer to tests at 50°C.

In their research on the effect of temperature on fatigue delamination growth Coronado et al. [8] found that delamination resistance increased with increasing temperature. Since they did not exclude fibre bridging and it was previously established that fibre bridging has a large influence on delamination resistance, it can be paraphrased that they found larger amounts of fibre bridging with increasing temperatures. This is in agreement with findings based on fracture mechanics in this research. Coronado et al. also based their results on fracture mechanics. Since Coronado et al. did not investigate a physical approach, the difference in findings between fracture mechanics and energy principles in this research project cannot be verified with their findings. All other past research projects into fatigue delamination growth in carbon fibre-epoxy laminates that were found took measures to exclude (the influence of) fibre bridging.

Since no record of research into fibre bridging development in fatigue delamination growth at different temperatures based on a physical approach was found, it is not possible to verify these conclusions. Therefore, additional research into the subject is recommended.

## 6.4 Temperature Influence on Stress Ratio Effect

When analyzing fatigue delamination resistance at different stress ratios using fracture mechanics, for all temperatures a clear stress ratio effect was found when both excluding and including fibre bridging into the analysis. It was found that fatigue delamination growth rate decreases with decreasing stress ratio. When excluding fibre bridging, this decrease was larger with decreasing temperature. When taking fibre bridging into account, this increase was smaller towards the extremities of the temperature interval (-40°C and 80°C). Since none of the previous researches into temperature effects in fatigue delamination growth make mention of using different stress ratios, these conclusions cannot be verified.

A stress ratio effect was also looked for using energy principles. Although less visible, a small stress ratio effect was found at all temperatures. The effect is bigger at more extreme temperatures both when excluding or including fibre bridging. When including fibre bridging is included the stress ratio effect is bigger compared to the zero bridging case.

As discussed in Subsection 2.6.1, a stress ratio effect is inherent to a one parameter model for analyzing fatigue delamination growth using fracture mechanics. In this research project, this one parameter is  $\Delta G$  and thus it is not surprising that a stress ratio effect was found. The change in this effect with temperature is impossible to be verified since no records of previous investigations were found.

In the energy based resistance curves, also a small change with stress ratio is observed. The change of this effect with temperature however is opposite compared to the fracture mechanics based effect. The fact that no previous research into the effect of temperature on the stress ratio effect has been found makes it difficult to make any definitive statements on whether one representation is more correct than the other. However, this lack of consistency can also be viewed as evidence that the stress ratio effect is not a stress ratio effect at all, but is in fact caused by other factors. In his PhD thesis [49], Amaral discovered that the shift in resistance curve believed to be the stress ratio effect has no connection to physical mechanisms but is purely due to the method of data representation. Following this reasoning, it is more evident that using a physical approach with energy principles does not yield the same results as the fracture mechanics based approach due to the lack of physical meaning. Yao [2] and Khan [51] did look for a physical meaning behind the stress ratio effect and they both concluded that a higher stress ratio leads to a rougher fracture surface which can explain the higher resistance to delamination at higher stress ratios. When keeping the findings of Amaral in mind, it may be that the observations by Yao and Khan are not caused by the stress ratio effect but have other causes like the high absolute values of applied load.

## 6.5 Temperature influence on fatigue delamination growth

When combining all of the above discussed parameters, the main research question "What is the influence of ambient temperature on fatigue delamination growth in composite laminates?" can be answered. Summarizing all different influences, using fracture mechanics as analysis method, it can be concluded that fatigue delamination resistance increases with increasing temperature. Thus, fatigue delamination growth decreases with increasing temperature. This is mainly influenced by the effect of temperature on fibre bridging since this seems to be the dominant parameter. When the stress ratio is changed, the delamination growth rate decreases with decreasing stress ratio.

In their research on the effect of temperature on fatigue delamination growth Coronado et al. [8] found that delamination resistance increased with increasing temperature. They did not exclude fibre bridging from their research. Sjörgen and Asp [63], found the opposite trend in their research as did Gregory and Spearing [62]. For the research of Gregory and Spearing, it was previously explained that they developed a model to exclude fibre bridging from their analysis, so therefore the different outcome is explained. For the research of Sjörgen and Asp, the different outcome can be explained as follows. For their research, they used a layup with a 5° and 0° interface where the crack occurred. With this interface, they observed almost no fibre bridging while maintaining properties close to unidirectional properties [63].

Considering the past research on fatigue delamination growth, this research is a good addition towards better understanding fatigue delamination growth. Whereas previous research excluded or included fibre bridging, during this research project both cases were analyzed. Therefore, it fills in a knowledge gap that could previously only be filled by comparing different researches.

When analyzing fatigue delamination growth in a physical way through energy principles, it was found that fatigue delamination resistance increased at both extremes of the temperature range investigated. Since no record of previous energy based research into the effect of temperature on fatigue delamination growth were found, it is not possible to verify this conclusion. Therefore, more research into this is recommended. This can be done by setting up a new experimental campaign of fatigue delamination tests at different temperatures or analyzing raw data from other research projects using energy principles. The added benefit of setting up a new experimental campaign is that with smaller temperature gaps, or by estimation the temperature at which the influence of temperature on fatigue delamination growth reverses.

# Conclusions and recommendations

In this chapter, conclusions are formulated based on the outcome of the research. Also, recommendations for future research are made.

## 7.1 Conclusions

The use of composites in aircraft has a specific set of challenges among which damage is one of the most critical. Damage that can not be visually detected from the outside is difficult to find in composite materials since they do not show signs of damage until the point of final failure. The research in this report focused on fatigue delamination, which is an internal damage type and thus difficult to notice. The effects of temperature on delamination growth are of great interest when designing aircraft since the materials inside an aircraft experience a whole range of temperatures during the aircrafts operational life. This research project aims to add to the knowledge of temperature effects on fatigue delamination growth and help fill in the knowledge gap that exists in the understanding of the effect of temperature on different parameters that influence fatigue delamination growth. In addition to the widely used fracture based approach for characterizing fatigue delamination growth, this research also uses an energy principles based physical approach.

To answer the main research question "What is the effect of ambient temperature on mode I fatigue delamination growth in composite laminates?" this research was structured around three sub-questions that each, when answered, provide information on a separate parameter that has influence on fatigue delamination growth.

When fibre bridging is excluded, fatigue delamination resistance was found to increase with decreasing temperature which means fatigue delamination growth decreases with decreasing temperature. This is supported by both fracture mechanics and energy principles based analysis.

Furthermore, it was found that fibre bridging has a large influence on fatigue delamination growth at all temperatures that were investigated. The amount of fibre bridging, and thus the magnitude of its effect on fatigue delamination growth, increases with increasing temperature.

To the contrary of room temperature results and past research, fibre bridging did not reach a final steady state. Steady states of fibre bridging occurred between certain delamination lengths, but fibre bridging kept increasing afterwards. This was found with both fracture mechanics analysis and energy principles analysis.

Using fracture mechanics analysis with similitude parameter  $\Delta G$ , where delta G is defined as  $(\sqrt{G_{max}} - \sqrt{G_{min}})^2$ , a clear stress ratio effect was found at all investigated temperatures. Fatigue delamination growth increases with increasing stress ratio. When excluding fibre bridging, this effect was larger with decreasing temperature. When taking fibre bridging into account, the influence on fatigue delamination growth became smaller towards the extremities of the temperature interval that was investigated. When using energy principles, fatigue delamination was also found to increase with increasing stress ratio. However, the influence of temperature on the stress ratio effect is opposite compared to the fracture mechanics case. This information, combined with insights from past research projects leads to the conclusion that there might not be a stress ratio effect and the phenomena attributed to this effect are caused by something else.

Combining all the information provided by answering the sub-research questions, it can be concluded that mode I fatigue delamination growth in composite laminates decreases with increasing temperature meaning an increase in fatigue delamination resistance with increasing temperature.

## 7.2 Recommendations

Based on the execution and outcome of this research project, the following recommendations for future research can be made.

For future research into the influence of temperature on fibre bridging, it is recommended to use longer specimens in order to be able to generate longer delaminations. This can provide more insight in if and when a second, higher level, stage of steady state fibre bridging occurs like the quasi-static resistance curves in this research seem to suggest.

A second recommendation is that more research is necessary using energy principles to create a better understanding on the physics behind the fatigue delamination phenomenon. This can be done by analyzing existing datasets or creating new datasets to be analyzed using energy principles.

Additional research into separate aspects of fatigue delamination growth is also recommended to create a better understanding of how different parameters influence fatigue delamination growth at different temperatures.

---

## References

- [1] H. Mahmood et al. Healable carbon fibre-reinforced epoxy/cyclic olefin copolymer composites. *Materials*, 13, 2020.
- [2] L. Yao. *Mode I Fatigue Delamination Growth in Composite Laminates with Fibre Bridging*. PhD thesis, TU Delft, 12 2015.
- [3] G.P. Thomas. Composites used in the aerospace industry. Accessed March 10, 2020.
- [4] Airbus. A350 xwb family. Accessed March 10, 2020.
- [5] Boeing. 787 dreamliner by design. Accessed August 28, 2020.
- [6] MechaniCalc inc. Fatigue crack growth. Accessed September 15, 2020.
- [7] Dictionary.com. Delamination. Accessed September 15, 2020.
- [8] P. Coronado et al. Influence of temperature on a carbon-fibre epoxy composite subjected to static and fatigue loading under mode-i delamination. *International Journal of Solids and Structures*, 49(21):2934–2940, 10 2012.
- [9] G. Charalambous et al. Temperature effects on mixed mode i/ii delamination under quasi-static and fatigue loading of a carbon/epoxy composite. *Applied Energy*, 77:75–86, 10 2015.
- [10] D. Ruffieux. Meteoswiss payerne cimo testbed2014-2015 report. Technical report, World Meteorological Organization, 2016.
- [11] M. Ros. World’s most extreme airports. Cited April 22, 2020.
- [12] J. Samenow. Temperatures in iranian city of ahvaz hit 129.2f (54c), near hottest on earth in modern measurements. *The Independent*, 6 2017. Retrieved from: <https://www.independent.co.uk/weather/iran-ahvaz-hottest-temperature-ever-recorded-world-record-extreme-death-valley-california-a7815771.html>.

- [13] R. Levinson et al. Potential benefits of solar reflective car shells: Cooler cabins, fuel savings and emission reductions. *Applied Energy*, 88(12):4343–4357, 12 2011.
- [14] R.J. Monaghan. Formulae and approximations for aerodynamic heating rates in high speed flight. Technical report, Royal Aircraft Establishment, 1987.
- [15] R.R. Heldenfels. Some design implications of the effects of aerodynamic heating. Technical report, National Advisory Committee for Aeronautics, 1955.
- [16] R. Sales et al. Influence of temperature on interlaminar fracture toughness of a carbon fibre-epoxy composite material. *Advanced Materials Research*, 1135:35–51, 1 2016.
- [17] Delta-tech. Matrix technical data sheet: Dt120 versatile high toughness epoxy matrix.
- [18] P. Coronado et al. Influence of low temperatures on the phenomenon of delamination of mode I fracture in carbon-fibre/epoxy composites under fatigue loading. *Composites Structures*, 112:188–193, 6 2014.
- [19] H. Wang et al. Experimental and numerical study of the interfacial shear strength in carbon fiber/epoxy resin composite under thermal loads. *International Journal of Polymer Science*, 2018, 2 2018.
- [20] J. Koyanagi et al. Time and temperature dependence of carbon/epoxy interface strength. *Composites Science and Technology*, 70:1395–1400, 9 2010.
- [21] J.A. Pascoe R.C. Alderliesten, R. Benedictus. Methods for the prediction of fatigue delamination growth in composites and adhesive bonds - a critical review. *Engineering Fracture Mechanics*, 112-113:72–96, 11 2013.
- [22] A.A. Griffith. The phenomena of rupture and flow in solids. *Philosophical Transactions of the Royal Society of London. Series A, Containing Papers of a Mathematical or Physical Character*, 221:163–198, 1921.
- [23] G.R. Irwin J.A. Kies. Fracturing and fracture dynamics. *Welding Journal Research Supplement*, 17:95s–100s, 2 1952.
- [24] S.K. Maiti. *Fracture Mechanics: Fundamentals and Applications*. Cambridge University Press, 2015.
- [25] G.R. Irwin. Analysis of stresses and strains near the end of a crack traversing a plate. *ASME Journal of Applied Mechanics*, 24:361–364, 9 1957.
- [26] H.M. Westergaard. Bearing pressures and cracks. *Journal of Applied Mechanics*, 6:A49–A53, 6 1939.
- [27] G.C. Sih P.C. Paris, G.R. Irwin. On cracks in rectilinearly anisotropic bodies. *International Journal of Fracture Mechanics*, 1:189–203, 9 1965.
- [28] A.T. Zehnder. *Fracture Mechanics*. Springer Netherlands, 2012.
- [29] T. Huang et al. Relationship between stress intensity factor and energy release rate of chinese-fir. *journal of tropical forest science*, 29:129–136, 2017.

- 
- [30] R.G. Forman V.A. Kearney, R.M. Engle. Numerical analysis of crack propagation in cyclic-loaded structures. *Journal of Basic Engineering*, 89:459–463, 9 1967.
- [31] G. Roderick et al. Debond propagation in composite reinforced metals. Technical Report NASA TM X-71948, NASA, 1974.
- [32] S. Mall G. Ramamurthy, M.A. Rezaizdeh. Stress ratio effect on cyclic debonding in adhesively bonded composite joints. *Composite Structures*, 8:31–45, 1987.
- [33] M. Shahverdi A.P. Vassilopoulos, T. Keller. Experimental investigation of r-ratio effects on fatigue crack growth of adhesively-bonded pultruded gfrp deb joints under ca loading. *Composites Part A: Applied Science and Manufacturing*, 43:1689–1697, 10 2012.
- [34] S. Mostovoy E. Ripling. Flaw tolerance of a number of commercial and experimental adhesives. *Adhesion Science and Technology*, 9:513–562, 1975.
- [35] C.G. Gustafson M. Hojo. Delamination fatigue crack growth in unidirectional graphite/epoxy laminates. *Journal of Reinforced Plastics and Composites*, 6:36–52, 1987.
- [36] D.R. Atodaria et al. Delamination growth behavior of a fabric reinforced laminated composite under mode i fatigue. *Journal of Engineering Materials and Technology*, 121:381–385, 7 1999.
- [37] M. Hojo et al. Effect of stress ratio on near-threshold propagation of delamination fatigue cracks in unidirectional cfrp. *Composites Science and Technology*, 29:273–292, 1987.
- [38] R. Khan. *Delamination Growth in Composites Under Fatigue Loading*. PhD thesis, TU Delft, 10 2013.
- [39] G. Roderick et al. Cyclic debonding of unidirectional composite bonded to aluminum sheet for constant-amplitude loading. Technical Report NASA TN D-8126, NASA, 1976.
- [40] C. Rans R.C. Alderliesten, R. Benedictus. Misinterpreting the results: How similitude can improve our understanding of fatigue delamination growth. *Composites Science and Technology*, 71:230–238, 1 2011.
- [41] R. Jones et al. Application of the hartmann-schijve equation to represent mode i and mode ii fatigue delamination growth in composites. *Composite Structures*, 94:1343–1351, 3 2012.
- [42] R. Khan R. Alderliesten, R. Benedictus. Two-parameter model for delamination growth under mode i fatigue loading (part:b model development). *Composites Part A: Applied Science and Manufacturing*, 65:201–210, 10 2014.
- [43] P. Paris M. Gomez, W.E. Anderson. A rational analytic theory of fatigue. *The trend in Engineering*, 13:9–14, 1961.
- [44] P. Paris. The fracture mechanics approach to fatigue. In *Proceedings of the 10th Sagamore Army Materials Research Conference*, pages 107–132, 1964.

- [45] R.F. Motta et al. Scrutinizing interlaminar fatigue loading cycle in composites using acoustic emission technique: Stress ratio influence on damage formation. To be published in *Composites Part A: Applied Science and Manufacturing* volume 138 (November 2020), 7 2020.
- [46] J.A. Pascoe et al. Using acoustic emission to understand fatigue crack growth within a single load cycle. *Engineering Fracture Mechanics*, 194:281–300, 5 2018.
- [47] A. Hartmann J. Schijve. The effects of environment and load frequency on the crack propagation law for macro fatigue crack growth in aluminium alloys. *Engineering Fracture Mechanics*, 1:615–631, 4 1970.
- [48] R.C. Alderliesten. How proper similitude can improve our understanding of crack closure and plasticity in fatigue. *International Journal of Fatigue*, 82:263–272, 5 2016.
- [49] L. Amaral. *Towards Fundamental Understanding of Interlaminar Ply Delamination Growth under Mode II and Mixed-Mode Loading*. PhD thesis, TU Delft, 10 2018.
- [50] J.R. Davis. *Gear Materials, Properties, and Manufacture*. ASM international, 2005.
- [51] R. Khan C. Rans, R. Benedictus. Effect of stress ratio on delamination growth behavior in unidirectional carbon/epoxy under mode i fatigue loading. *ICCM17*, 2009.
- [52] J. Jia J.F. Davalos. Study of load ratio for mode-i fatigue fracture of wood-frp-bonded interface. *Journal of Composite Materials*, 38:1211–1230, 2004.
- [53] R. Alderliesten. Fatigue delamination of composite materials – approach to exclude large scale fibre bridging. *IOP Conference Series: Materials Science and Engineering*, 388, 2018.
- [54] W.S. Johnson P. Mangalgiri. Investigation of fiber bridging in double cantilever beam specimens. *Journal of Composites Technology and Research*, 2 1987.
- [55] W.L. Bradley R.N. Cohen. Matrix deformation and fracture in graphite-reinforced epoxies. pages 389–410. American Society for Testing and Materials, 1985.
- [56] R. Khan et al. Experimental investigation of the microscopic damage development at mode i fatigue delamination tips in carbon/epoxy laminates. *Jurnal Teknologi*, 78, 11 2016.
- [57] M. Hojo et al. Modes i and ii interlaminar fracture toughness and fatigue delamination of cf/epoxy laminates with self-same epoxy interleaf. *International Journal of Fatigue*, 28:1154–1165, 10 2006.
- [58] L. Yao et al. A validation of a modified paris relation for fatigue delamination growth in unidirectional composite laminates. *Composites Part B: Engineering*, 132:97–106, 1 2018.
- [59] L. Yao et al. Fibre bridging effect on the paris relation of mode i fatigue delamination in composite laminates with different thicknesses. *International Journal of Fatigue*, 103:196–206, 10 2017.

- 
- [60] B.F. Sorensen T.K. Jacobsen. Large-scale bridging in composites: R-curves and bridging laws. *Composites Part A*, 29A:1443–1451, 1998.
- [61] Jacobsen et al. Modelling of r-curves from measured bridging laws. In *IUTAM Symposium on Analytical and Computational Fracture Mechanics of Non-Homogeneous Materials*, 2001.
- [62] J.R. Gregory S.M. Spearing. A fiber bridging model for fatigue delamination in composite laminates. *Acta Materialia*, 54:5493–5502, 11 2004.
- [63] A. Sjörgen L.E. Asp. Effects of temperature on delamination growth in a carbon/epoxy composite under fatigue loading. *International Journal of Fatigue*, 24:179–184, 2002.
- [64] W.S. Chan A.S.D. Wang. Free-edge delamination characteristics in s2/ce9000 glass/epoxy laminates under static and fatigue loads. In P.A. Lagace, editor, *Composite Materials: Fatigue and Fracture*, pages 270–295. American Society for Testing and Materials, Philadelphia, 1998.
- [65] C.D. Rans R.C. Alderliesten, R. Benedictus. Predicting the influence of temperature on fatigue crack propagation in fibre metal laminates. *Engineering Fracture Mechanics*, 78:2193–2201, 4 2011.
- [66] I.A. Ashcroft et al. Effect of temperature on the quasi-static strength and fatigue resistance of bonded composite double lap joints. *Journal of Adhesion*, 75:61–88, 2001.
- [67] I.A. Ashcroft S.J. Shaw. Mode i fracture of epoxy bonded composite joints 2. fatigue loading. *International Journal of Adhesion and Adhesives*, 22:151–167, 10 2002.
- [68] ASTM International. Standard test method for mode i interlaminar fracture toughness of unidirectional fiber-reinforced polymer matrix composites.
- [69] A.J. Brunner R.C. Alderliesten. Determination of mode i fatigue delamination propagation in unidirectional fibre-reinforced polymer composites. version 3.1.



---

Appendix A

---

## **List of experiments**

**Table A.1:** List of all experiments performed in this research project

Test ID	Specimen ID	Load case	Laminate layup	Temperature	Stress ratio
QS_UD_-40_01	UD_010	Quasi-static	UD	-40°C	/
QS_UD_-40_02	UD_008	Quasi-static	UD	-40°C	/
QS_UD_-40_03	UD_009	Quasi-static	UD	-40°C	/
QS_UD_RT_01	UD_002	Quasi-static	UD	Room temperature	/
QS_UD_RT_02	UD_015	Quasi-static	UD	Room temperature	/
QS_UD_RT_03	UD_113	Quasi-static	UD	Room temperature	/
QS_UD_50_01	UD_004	Quasi-static	UD	50°C	/
QS_UD_50_02	UD_006	Quasi-static	UD	50°C	/
QS_UD_50_03	UD_007	Quasi-static	UD	50°C	/
QS_UD_80_01	UD_011	Quasi-static	UD	80°C	/
QS_UD_80_02	UD_012	Quasi-static	UD	80°C	/
QS_UD_80_03	UD_014	Quasi-static	UD	80°C	/
F0.1_UD_-40_01	UD_022	Fatigue	UD	-40°C	0.1
F0.1_UD_-40_02	UD_114	Fatigue	UD	-40°C	0.1
F0.5_UD_-40_01	UD_112	Fatigue	UD	-40°C	0.5
F0.5_UD_-40_02	UD_115	Fatigue	UD	-40°C	0.5
F0.1_UD_RT_01	UD_017	Fatigue	UD	Room temperature	0.1
F0.1_UD_RT_02	UD_104	Fatigue	UD	Room temperature	0.1
F0.5_UD_RT_01	UD_102	Fatigue	UD	Room temperature	0.5
F0.5_UD_RT_02	UD_111	Fatigue	UD	Room temperature	0.5
F0.1_UD_50_01	UD_020	Fatigue	UD	50°C	0.1
F0.1_UD_50_02	UD_103	Fatigue	UD	50°C	0.1
F0.5_UD_50_01	UD_107	Fatigue	UD	50°C	0.5
F0.5_UD_50_02	UD_110	Fatigue	UD	50°C	0.5
F0.1_UD_80_01	UD_101	Fatigue	UD	80°C	0.1
F0.1_UD_80_02	UD_105	Fatigue	UD	80°C	0.1
F0.5_UD_80_01	UD_108	Fatigue	UD	80°C	0.5
F0.5_UD_80_02	UD_109	Fatigue	UD	80°C	0.5